

Fault mesh petroleum plays in the Donghetang area, Tabei Uplift, Tarim Basin, NW China, and its significance for hydrocarbon exploration

Qiang Liu<sup>1,2</sup>, Huaimin Xu<sup>1</sup>, Zhicheng Lei<sup>3,4</sup>, Zhongchao Li<sup>5</sup>, Yunbin Xiong<sup>5</sup>, Songze Li<sup>5</sup>, Bobo Luo<sup>5</sup>, Daoyuan Chen<sup>5</sup>

<sup>1</sup>Department of Geoscience, China University of Petroleum (Beijing), Beijing 102249, China

<sup>2</sup>Institution of Petroleum Exploration and Development of SW Tarim Basin, Tarim Oilfield Company, PetroChina, Korla 841000, China

<sup>3</sup>Jiangxi Engineering Laboratory on Radioactive Geoscience and Big data Technology, East China University of Technology, Nanchang 330013, China

<sup>4</sup>Jiangxi Engineering Technology Research Center of Nuclear Geoscience Data Science and System, East China University of Technology, Nanchang 330013, China

<sup>5</sup>Research Institution of Petroleum Exploration and Development, Zhongyuan Oilfield Company, Sinopec, Puyang, Henan, 457300, China

\*Corresponding author contact detail, E-mail: oasis\_1996@163.com

**Abstract:** The hydrocarbon formation mechanism and potential targets in clastic strata from the Tabei Uplift, Tarim Basin, are documented using the fault mesh petroleum plays theory based on integrating seismic, well log, well core and geochemistry data. The reservoirs in the Donghetang area are typical allochthonous and far source fault mesh petroleum plays. There are two sets of fault meshes in the study area, the Donghe sandstone and Permian and Triassic strata combination as well as the fourth and third formation combination, in the Jurassic strata. The fault mesh petroleum play in the Jurassic is a secondary reservoir that originates from the Carboniferous Donghe sandstone reservoir adjustment based on source correlation. The fault mesh carrier systems are divided into four styles, which include the fully-connected, fault-unconformity-transient storage relay, fault-transient storage-unconformity relay and transient storage-fault relay styles, according to the architecture of the fault mesh. Based on the characteristics of the fault mesh petroleum plays, the reservoirs are divided into three categories, including an upper-transient storage, inner-transient storage, and margin-transient storage styles, and 15 styles of those reservoirs. Integrated analysis of the hydrocarbon generation and faulting time periods reveals that there were four periods of hydrocarbon charging, with the first three stages charging the reservoirs with oil and the last stage charging the reservoirs with gas. There are multiple stages of reservoir accumulation and adjustment in the fault mesh in the study area. These multiple stages of fault mesh accumulation and adjustment are the main reason that the reservoir distribution multiple vertical units have different hydrocarbon properties. Fault-block reservoirs and lithologic reservoirs related to the inner-transient storage and upper-transient storage styles are the main exploration targets in the clastic strata in the study area.

**Keywords:** Allogenic and far source accumulation; Fault mesh petroleum plays; Multiple accumulation and adjustment; Tabei Uplift; Tarim Basin; NW China

## 1 Introduction

Dow first proposed the 'oil system' concept in 1972, and related concepts were subsequently described (Dow, 1974; Perrodon, 1983,1992; Demaison, 1984; Meissner, 1984; Ulmishek, 1986; Magoon, 1988, 1992). This work gave birth to the petroleum system concept that was described in the AAPG Memoir 60 (Magoon & Dow 1994). A 'petroleum system' comprises a pod of mature source rock and all of the migration paths, reservoir rocks, caprocks and traps that can be charged by that source rock to produce oil and gas accumulations.

Chinese geologists that applied the concepts of the petroleum system found that it wasn't suitable for hydrocarbon exploration in the complex superimposed basins in NW China (Pang et al., 2003, 2010). Some studies proposed source control theory (Hu et al., 1986) and hybrid petroleum systems (Zhao and He, 2000) according to the reservoir formation characteristics in the superimposed basins. Jin et al. (2004) described the concept of a petroleum accumulation system, which uses the reservoir as a key unit of study. The concept of the petroleum accumulation system emphasizes that reservoir formation relies on efficient allocation of all of the hydrocarbon formation units to form a reservoir. Xu et al. (2008) divided the petroleum accumulation system into three types following the origin of a source-reservoir-cap and its assemblage, which include allogenic, authigenic and hybrid hydrocarbon source petroleum accumulation systems.

Zhang et al. (2003, 2004) proposed the concept of fault mesh petroleum plays based on research on reservoir-forming processes of secondary reservoirs in the Jiyang Depression, Bohai Bay Basin, eastern China. A well-defined fault mesh petroleum play usually contains three basic elements, a hydrocarbon source network at the base, a transient storage for migrating hydrocarbons in the middle, and a petroleum accumulation network at the top (Zhang et al., 2003, 2004). The mesh that contains the oil source network at the base consists of primary faults and (or) regional unconformities in direct contact with mature hydrocarbon source beds, and secondary faults that intercept lenticular sandstones. The transient storage is a sheet-like, thick, porous sandstone deposits. The fault mesh petroleum play is the allogenic hydrocarbon that was generated in the lower strata and migrated through the oil source network, temporarily accumulated in the transient storage and migrated once more vertically or laterally into shallower reservoirs. Such a play concept stresses the role of faults in the transmission of petroleum fluids from relatively deeply buried source rocks to suitable petroleum host rocks and traps in the stratigraphically younger strata (Wang et al., 2005). The accumulation processes of fault mesh petroleum plays were proven by physical simulations (Zhang et al., 2003, 2004). Zhang et al. (2013) divided the fault mesh petroleum plays into far-source and near-source styles according to the relationship between the petroleum accumulation system and the source rock.

Many studies have focused on the reservoir formation in the Tabei Uplift, Tarim Basin, for oil source correlation, hydrocarbon accumulation stages and reservoir formation mechanisms (Li et al., 1996; Zhang et al., 2000; Zhu et al., 2013; Li et al., 2016). There are two viewpoints on the origin of the Jurassic condensate reservoirs in the study area: Zhang et al. (2012) proposed that the condensate reservoirs are hybrids from marine and continental hydrocarbons, and Liang et al. (1998) suggested that the condensate reservoirs originated from marine hydrocarbons, which resulted from hydrocarbon adjustment. Commonly, the Carboniferous and Jurassic reservoirs were studied as separate petroleum accumulation systems, and the reservoir formation mechanism from a local to regional scale is rarely discussed. This study applies the fault mesh petroleum play theory to analyze the reservoir formation mechanism and accumulation patterns during hydrocarbon generation periods, faulting stages and transient storage, and predict exploration targets and beneficial zones in the study area.

## **2 Data and methods**

Seismic attributes from the seismic data in the depth domain were analyzed to understand the reservoir distribution of the transient storage and petroleum accumulation network during the Jurassic. Cored material of 2686 and 180 samples in the Donghe sandstone and Jurassic strata, respectively, were used to analyze the petrophysical properties of the transient storage and petroleum accumulation network. The architecture of the unconformity complex between the Jurassic and lower strata was determined by well correlation. Geochemistry parameters and light hydrocarbon compositions from 11 wells from the Donghe sandstone and 6 wells from the Jurassic strata were used to analyze the source relationship between the Donghe sandstone and Jurassic

reservoirs, which determined the n-alkanes distribution and light hydrocarbon composition.

Gas compositions were measured using an Agilent 7890 gas composition instrument, which was equipped with four valves, six packed columns, a flame ionization detector (FID) and two thermal conductivity detectors (TCD). The oven temperature was held at 50 °C, and the FID temperature remained at 80 °C.

The gas chromatography (GC) was performed using an Agilent 6890A gas chromatograph equipped with a fused silica column (HP-PONA, 50 m×0.20 mm i.d. ×0.5 mm film thickness) and a FID at 300 °C. The experimental methods of the GC were described in detail by Song et al. (2016). The urea complexation method was used to separate the n-alkane and UCM from the oil-saturated hydrocarbons.

The bulk composition: the oil was extracted by washing the oil sand with chloroform, and the bulk composition including alkane, asphalt, aromatic and resin was separated using silica gel column chromatography.

The software 2DMove was used to balance two cross sections and analyze fault evolution processes and timing of the Paleozoic faults. Flexural slip was used to maintain stratigraphic thickness and fault parallel flow was used during fault restoration.

### 3 Geological setting

The Tarim Basin lies between the Chinese Tianshan Mountains to the north and western Kunlun Mountains to the south and is confined by the Altun Mountains to the southeast (Fig. 1A, B). The Tabei Uplift is located between the Kuche and Manjiaer depressions in the Tarim Basin. The Donghetang tectonic belt is located at the northern Halahatang sag, in the middle of the Tabei Uplift (Fig. 1C). It consists of five Carboniferous Donghe sandstone reservoirs (DH1, DH4, DH5, DH6, DH14) and a Jurassic condensate reservoir (Fig. 1D).

#### 3.1 Petroleum geological setting

The strata from the Ordovician through the Quaternary were drilled in the study area. Fig. 2 shows the sedimentary basin fill and stratigraphic framework in the study area. The Donghe sandstone is a diachronous unit that spans from the Devonian to the Carboniferous (Wang et al., 2004). We use the term Carboniferous Donghe sandstone in this paper for convenience. There is an onlapped unconformable surface with the Silurian at the bottom and a truncation unconformable surface with the Permian and Jurassic at the top of the section.

The Donghe sandstones of the DH1 reservoir in burial history characterized by long-term in shallow buried depth and short-term deeply buried (Fig.3), it was uplifted to the surface and eroded in the Late Hercynian period, and continue subsidence in the Early Cretaceous, and then fast subsidence to the present buried depth range from 5700 to 6000m in the Hiyama period. Reservoir temperature from the well DH1 in the Donghe sandstones at 5718m is 140°C.

Previous work suggests that in the study area, the Donghe sandstone was deposited in a shoreline environment and is a thick fine-grained quartz sandstone (Li et al., 2016). The average thickness of the Donghe sandstone is approximately 250 meters and can be divided into 10 sand sets on the basis of analyzing sequence stratigraphy (Fig. 2). The hydrocarbon source rocks are Ordovician marine carbonate rocks from the southern Manjiaer Depression (Zhang et al., 2000; Chang et al., 2013).

The Jurassic and its contact with older strata form a high-angle unconformity, and a parallel unconformity with the Cretaceous. The Lower Jurassic can be divided into two formations, which include the  $J_{IV}$  and  $J_{III}$ , from bottom to top. The sedimentary depositional system of the  $J_{IV}$  formation is a braided river environment and it is distributed widely in the study area (Fig. 4C). The  $J_{III}$  formation was deposited by an alluvial fan and is distributed in the northern and northwestern part of the study area (Fig. 4D).

The regional seal includes a Carboniferous bioclastic limestone and mudstone assemblage, and a thick lacustrine mudstone in the Middle-to-Upper Jurassic. There are two petroleum accumulation assemblages: the

lower assemblage is a Carboniferous Donghe sandstone, bioclastic limestone and mudstone, and the upper assemblage is the  $J_1$  formation and  $J_{2-3}$  formation. The reservoir properties are significantly different between the lower and upper assemblages, with the former being a crude oil reservoir, and the latter a condensate reservoir.

### 3.2 Structure evolution

There are two fault systems in the study area, a thrust and strike-slip fault system that was active in the Paleozoic and an extensional fault system active in the Mesozoic and Cenozoic. The thrust faults strike in a NE-SW direction and the strike-slip faults are right-lateral and strike in a NW-SE direction (Fig. 1D). The normal fault system in the Jurassic consists of echelon faults in a NE direction (Fig. 1F).

The ancient uplift formed in the Early Hercynian, and the fault activity reached a maximum during the Middle to Late Hercynian (Tang et al., 1999), volcanic activity occurred in the Permian to Early Triassic and the Paleozoic structural framework was set in the Late Triassic (Liu et al., 2012). The faults F1 and F5 (Fig. 5) were still active in the Jurassic to Cretaceous due to the strong activity of the Tianshan thrust fault zones (Tang et al., 2012). The extensional fault system formed in the Neogene because of earlier Kuche foreland frontal uplift in the northern part of the study area (Wei et al., 2001).

Generally, during the Devonian to the Triassic there was an intense thrust and uplift stage and fault activity reached the maximum during the Permian to Triassic, which is why Permian and Triassic strata were eroded. The study area began to subside in the Jurassic, which resulted in a regional high angle unconformity between the Jurassic and older strata (Fig. 1F). There was weak thrust activity during the Jurassic to Cretaceous. The thrust faults in the Paleozoic were reactivated due to negative inversion during the Eocene to Miocene (Chen et al., 1998; Tang et al., 1999; Cheng et al., 2009). During this final stage, the strata inclination in the study area experienced inversion due to the subsidence of the northern Kuche Depression, which resulted in a structural high that migrated from north to south, affecting the Jurassic and its overlying strata (Fig. 5).

## 4 Results

### 4.1 The characteristics of fault mesh

#### 4.1.1 The transient storage

The petrophysical properties of the Donghe sandstone reservoir in the middle sand sets of 2 to 5 with permeabilities 4 to 8 times larger than at both ends but little change in porosity, according to an analysis of 2686 samples from well cores (Fig. 6A). The permeability in the sand sets 0 to 8 is range from 1 md to 50 md, 0.4 md to 200 md, 0.1 md to 400 md, 0.4 md to 500 md, 0.4 md to 300 md, 0.2 md to 700 md, 0.5 md to 250 md, 0.2 md to 70 md, 0.1 md to 20 md, respectively, and the average of that is 31.4 md, 15.6 md, 88.1 md, 167.3 md, 79.5 md, 93.65 md, 38.98 md, 8.82 md and 8.91 md, respectively. The average porosity is 15% and range from 3% to 21% in the Donghe sandstone. The average permeability is 360 md and the average porosity is 18.6% in the  $J_{IV}$  formation, according to an analysis of 42 samples from well core data (Fig. 6B).

The transient storage occurred over a relatively large geographic area in a porous, well connected and thick sheet-like sandstone reservoir (Zhang et al., 2003, 2004). These sandstones serve as temporary storage spaces, through which deep-sourced petroleum fluids migrate, either laterally or vertically, into shallower reservoirs (Zhang et al., 2003, 2004). Although the concept of fault mesh petroleum plays proposed under the geological setting of shallow burial depth (less than 2000m) and high petrophysical properties (with average porosity value 35.3% and permeability value 1500 md), compared with that the reservoirs are deeply buried (below 5000m) and low petrophysical properties. While following Zhang et al. (2003,2004), the key for hydrocarbon accumulation of that system is the well-development transient storage, which is sheet-like, thick, well-connected porous sandstone deposits, and widely spread. According to that concepts, there are two sets of transient storage reservoirs in the

study area, which include the shoreline facies of the Carboniferous Donghe sandstone, a sandstone reservoir with an average thickness of 250 meters, and braided river deposits of the  $J_{IV}$  formation, a sandstone reservoir with an average thickness of 10 meters (Fig. 7).

#### **4.1.2 The petroleum accumulation network**

The petroleum accumulation network upper the transient storage provides suitable reservoirs for hydrocarbon accumulation (Zhang et al., 2003, 2004). There are two sets of petroleum accumulation networks, which include continental deposits from the Permian to the Triassic, and alluvial fan deposits in the  $J_{III}$  formation. The average permeability is 45 md and the average porosity is 16.5% in the Jurassic petroleum accumulation network of the  $J_{III}$  formation, according to 138 samples from the well core (Fig. 7B). No hydrocarbon have been found in the Permian-Triassic in the drilled wells, and the hydrocarbon distribution widely in the  $J_{III}$  formation according to the well-logging interpretation and well test (Fig. 4 D). The thin sandstone reservoirs in the thick lacustrine mudstone of  $J_{2-3}$  can also be part of the petroleum accumulation network.

#### **4.1.3 The hydrocarbon source network**

The hydrocarbon source network provides fairways for hydrocarbons generated in a deep source to migrate vertically upward to shallow strata, and often consists of primary faults and/or regional unconformities in direct contact with mature petroleum source beds, and secondary faults intercepting lenticular fluvial sandstones (Zhang et al., 2004). The hydrocarbon source rocks are marine Ordovician source rocks in the southern study area of the Manjiaer Depression (Zhu et al., 2013; Huang et al., 2016). The hydrocarbon accumulation in the Carboniferous Donghe sandstone and Jurassic reservoirs that originated from the Ordovician source rocks must have migrated through the hydrocarbon source network.

The hydrocarbon source network is divided into a fully-connected style and a lower-connected style according to the time-space relationships between the faults, unconformity and two sets of transient storage units in the study area. The fully-connected style of the hydrocarbon source network means that the two sets of transient storage are connected with the hydrocarbon source rocks by faults, an unconformity and/or a sandstone reservoir (Fig. 8). The lower-connected style of the hydrocarbon source network means that just the transient storage of the Carboniferous Donghe sandstone is connected with the hydrocarbon source rocks by faults and/or an unconformity, and the second transient storage is not connected with those faults and/or unconformity (Fig. 8).

The faults that have been active a long time in the northern study area, such as faults F5 and F1, and the unconformity between the Jurassic and Carboniferous, constitute the fully-connected style of the hydrocarbon source network. The faults that formed during the Carboniferous to Triassic constitute the lower-connected style of the hydrocarbon source network and are primarily distributed in the middle part of the study area.

The small-scale extensional faults in the Jurassic are not directly connected with the Ordovician source rocks, but can serve as hydrocarbon migration channels for petroleum accumulation network of the  $J_{III}$  formation. The hydrocarbon from the  $J_{IV}$  reservoirs and Carboniferous Donghe sandstone reservoirs migrated along extensional faults to the  $J_{III}$  formation and accumulated.

### **4.2 Physical properties and geochemistry composition of crude oil**

The reservoirs of the Carboniferous Donghe sandstone and Jurassic include crude oil, heavy oil and condensate oil. The crude oil density, viscosity, sulfur content and saturated hydrocarbons are similar between the Donghe sandstone reservoir and the Jurassic reservoir, and range from 0.76 to 0.92 g/cm<sup>3</sup>, 5 to 13 mPa·s, 0.2% to 1% and 25% to 72%, respectively. The viscosity of the condensate reservoir in the Jurassic ranges from 0.8 to 1.5 mPa·s. The ratio of the saturated to aromatic hydrocarbons in the Donghe sandstone reservoir ranges from 2 to 7, and from 1.6 to 2.8 in the Jurassic reservoir (Table 1).

The value of the odd-even predominance (OEP) and carbon preference index (CPI) is approximately 1, and the value of Ph/nC<sub>18</sub> and Pr/Ph in the Donghe sandstone and Jurassic reservoir are similar, ranging from 0.35 to

0.7, and less than 1, respectively. The value of Pr/nC<sub>17</sub> in the Donghe sandstone reservoir ranges from 0.3 to 0.8, and from 0.2 to 0.4 in the Jurassic reservoir (Table 2).

### 4.3 The natural gas composition and light hydrocarbon composition

The Donghe sandstone natural gas is characterized by high CO<sub>2</sub>, N<sub>2</sub> and high relative density between 18% and 32%, 20% and 36%, and 0.8 to 1.2, respectively. The Jurassic is naturally characterized by high methane content and a low relative density, between 82% and 87%, and less than 0.7, respectively (Table 3).

The content of n-alkanes and aromatics in the light hydrocarbon composition between the Donghe sandstone and Jurassic reservoir is similar, between 35% to 50% and 0.3% to 16%, respectively. The content of the isoalkane and cycloalkane in the Jurassic reservoir is high, between 26% to 36% and 9% to 19%, respectively. The content of those in the Donghe sandstone reservoir is low, between 12% to 31% and 0.2% to 15%, respectively (Table 4).

## 5 Discussion

### 5.1 The origin of the Donghe sandstone and Jurassic hydrocarbon

Mango (1987; 1990b) suggested that the K1 values of hydrocarbons in same source are basically consistent, and the K1 value defined as the ratio of sum of concentrations of (2-methylhexane+2,3-dimethylpentane) to (3-methylhexane+2,4-dimethylpentane). The K1 value of the gas in the Donghe sandstone and the Jurassic reservoir is relatively consistent, ranging from 1.03 to 1.16 (Table 4, Fig. 9), indicating that the natural gas in the Donghe sandstone and the Jurassic reservoirs originated from the same source rocks.

The Donghe sandstone reservoir hosts a marine hydrocarbon and originates from an E-O source rocks in the southern study area, the Manjiaer Depression (Zhu et al., 2013; Chang et al., 2013; Zhang et al., 2000, 2002; Cheng et al., 2016; Huang et al., 2016), which indicates that the Donghe sandstone reservoir has a typical allogenic and far source accumulation. The condensate reservoirs in the Tabei Uplift can be divided into continental facies and marine facies. The former is characterized by the heavy value of carbon isotope of ethane (-25.4‰--22.05‰), the values of Pr/Ph are more than 2, and both the values of Pr/nC<sub>17</sub> and Ph/nC<sub>18</sub> are less than 0.2. In contrast, the latter is characterized by a light value of carbon isotope of ethane (-28‰--37‰), the value of Pr/Ph is less than 1.2, and both the values of Pr/nC<sub>17</sub> and Ph/nC<sub>18</sub> are more than 0.2 (Liang et al., 1998; Zhang et al., 2010; Liu et al., 2009). The values of Pr/Ph are less than 1, and both the values of Pr/nC<sub>17</sub> and Ph/nC<sub>18</sub> are more than 0.2 in crude oil, heavy oil, asphaltic sand and oil sand in the Donghe sandstone and the Jurassic reservoirs, which indicate that the hydrocarbon in the Donghe sandstone and the Jurassic reservoirs originate from the same source rocks.

Wang et al. (2008) proposed that when i/nC<sub>4</sub> is less than 0.9, gas could form in three different conditions: the gas is mixed from liquid hydrocarbon cracking and kerogen degradation in a closed system when i/nC<sub>5</sub> < 0.6, from hydrocarbon cracking when i/nC<sub>5</sub> ranges from 0.6 to 0.85, from kerogen degradation when i/nC<sub>5</sub> > 0.85. Since i/nC<sub>4</sub> in the Donghe sandstone and Jurassic reservoirs is less than 0.9, and i/nC<sub>5</sub> ranges between 0.39 and 0.91 in the Donghe sandstone reservoir and less than 0.6 in the Jurassic reservoir (Table 4), the gases in the Donghe sandstone reservoir are derived from both kerogen degradation and liquid hydrocarbon cracking and the gases in the Jurassic reservoir are derived from liquid hydrocarbon cracking.

### 5.2 Time-space collocation between the fault mesh and hydrocarbon generation

Detailed hydrocarbon accumulation periods of the Carboniferous Donghe sandstone and Jurassic reservoirs in Tabei Uplift were described by Zhang et al. (2012), Wang et al. (1997), and Zhang et al. (2006). The reader should refer to their papers for more detailed information. Based on an integrated analysis of previous research and the same source rocks of the Donghe sandstone and the Jurassic reservoir, we proposed that there were four

stages of hydrocarbon charge of the clastic rock reservoir. The first stage occurred during the Late Permian to Early Triassic with oil charge, the second stage occurred during the Late Jurassic to Late Cretaceous (151-85.8 Ma) with oil charge, the third stage occurred during the Eocene (50-40 Ma), and the fourth stage occurred during the Miocene (20 Ma) to present day with a gas charge.

Faults serve as the main unit in the source network. During faulting they acted as conduits for hydrocarbon migration and during the static stage, they acted as barriers (Hooper, 1991; Knipe, 1997; Indrevær et al., 2014). The active faults during the hydrocarbon generation stage can be conduits for hydrocarbon migration. The faults that formed after the hydrocarbon generation stage are significant for petroleum accumulation in the petroleum accumulation network and hydrocarbon adjustment of the transient storage reservoirs. The faults that formed before hydrocarbon generation are barriers to hydrocarbon migration.

According to the time-space collocation between the fault and hydrocarbon generation (Fig. 10), the faults F1 and F5 were active for the longest time and correlate well with four periods of hydrocarbon generation. The faults also connected two transient storages of the Donghe sandstone and  $J_{IV}$  braided river deposits, and constitute the fully-connected hydrocarbon source network with an unconformity between Jurassic and older strata. The faults F2, F3, F4, F9, F10, F11 and F12 form the lower connected hydrocarbon source network and only connect the Donghe sandstone and Ordovician source rocks. According to the relationship between the faulting and hydrocarbon generation stages of faults F6, F7 and F8, these faults migrated the hydrocarbon to the Donghe sandstone transient storage traps during structure inversion period.

The extensional faults that formed during the Eocene to Miocene and cut Triassic strata help migrate the hydrocarbon that accumulated in the  $J_{IV}$  transient storage to the  $J_{III}$  petroleum accumulation network. The faults can also serve as a minor hydrocarbon source network with a fully-connected hydrocarbon source network that migrates the hydrocarbon generated during the Eocene to Miocene to the traps and accumulates.

### **5.3 The reservoir models of fault mesh petroleum plays in the study area**

The reservoirs in the study area are typical allogenic and far source accumulation, such that the reservoir forms only when hydrocarbon migrated by faults and unconformities constitutes the hydrocarbon source network. The carrier system of the fault mesh can be divided into four styles according to the characteristics of fault mesh petroleum plays, which include fully-connected style (Fig. 11a), fault-unconformity-transient storage relay style (Fig. 11b), fault-transient storage-unconformity relay style (Fig. 11c), and transient storage-fault relay style (Fig. 11c). Integrating the fault mesh characteristics and spatial relationships between the reservoir and transient storage, the reservoirs related to the fault mesh can be divided into inner-transient storage reservoirs, upper-transient storage reservoirs and margin-transient storage reservoirs (Fig. 12).

#### **5.3.1 The model of reservoirs upper-transient storage**

The reservoirs described as upper-transient storage are located in the upper transient storage, which is a reservoir in the petroleum accumulation network that includes drape anticline, fault-block, and stratigraphic reservoirs (Fig. 12a-c). The carrier system is a transient storage-fault relay style. The hydrocarbon that accumulated in the transient storage migrated along faults to the traps in the petroleum accumulation network. The lava-shielded reservoir may exist because of strong volcanic activity during the Permian to Early Triassic (Liu et al., 2012).

#### **5.3.2 The model of reservoirs inner-transient storage**

The reservoirs described as inner-transient storage are located in the interior transient storage and are mainly anticline (Fig. 12f, g, i) and fault-block reservoirs (Fig. 12e). Lava-shielded reservoirs may exist in the transient storage of the Donghe sandstone. Stratigraphic reservoirs, such as sandbank lens (well DH1-5-5), up-dip pinch-out sandstone and channelized sandstone reservoirs (Fig. 12k), may exist in the transient storage of the  $J_{IV}$  braided river deposits (Fig. 12h), in which hydrocarbon migrated by a fully-connected hydrocarbon source network

style (Fig. 11a), a fault-unconformity-transient storage relay style (Fig. 11b) or a fault-transient storage-unconformity-transient storage relay style (Fig. 11c) to the transient storage traps and accumulated.

### **5.3.3 The model of reservoirs margin-transient storage**

The reservoirs described as margin-transient storage are located in the margin of the transient storage and are mainly related to the unconformity. There are three layers in the unconformity complex, including the rocks above the unconformity interface, a weathered clay and paleokarst zone, and a different composition that can form a different reservoir type (Martinsen, 2003a, b; He et al., 2007). Simulation experiments show that weathered clay is the key part in the formation reservoirs for the unconformity-related hydrocarbon reservoirs (Wu et al., 2009). According to the stratigraphic contact relationships, the reservoirs related to the regional unconformity between the Jurassic and older strata were divided into buried-hill-reservoirs (Fig. 12l), truncate-reservoirs (Fig. 12m), erosional-remnant-reservoirs (Fig. 12n), and stratigraphic-reservoirs (Fig. 12o), where the sandstone fills up a local low in the paleotopography.

The truncate-reservoirs may not exist in the study area because the basal conglomerate above the unconformity interface between the Jurassic and Carboniferous is 3 to 5 meters thick which is widely distributed, according to well data (Fig. 7). The failed exploration well DH2 and DH3 that tested the unconformity reservoir also indicates that the targets are high risk. The drilling results of well DH22 show that a thick lacustrine mudstone sits above the unconformity interface between the Jurassic and the Pre-Carboniferous, meaning buried-hills-reservoirs may exist in the study area. Erosional-remnants formed by differential weathering in the Jurassic strata, and the hydrocarbon migrated to the traps by a fault-unconformity relay style, such as the DH12 reservoir in the Jurassic.

## **5.4 The process of fault mesh petroleum plays from Carboniferous to Jurassic in the study area**

Based on an integrated analysis of the faulting and hydrocarbon generation, there are four periods of hydrocarbon generation and multiple hydrocarbon reservoirs adjustments. Below, the DH1 Oilfield is used as an example to elaborate on the process of the formation of fault mesh reservoirs. Three times hydrocarbon charged history can be concluded following Zhang et al., (2012) and Zhang & Luo (2012) who had been used the homogenization temperature of salt water inclusions associated with hydrocarbon inclusions in the well DH11 and K-Ar dating of authigenic illite of Devonian sandstone reservoirs in the well Ha6 from the Halahatang sag, respectively (Fig.3). The timing of hydrocarbon charging are following in order: Late Permian to Early Triassic charged with hydrocarbon oil, Jurassic to Cretaceous charged with hydrocarbon oil and Late Neogene charged with hydrocarbon gas originated from underlying liquid hydrocarbon cracking and kerogen degradation (Zhang et al., 2002; Zhu et al., 2013; Lei et al., 2019) in which we divided it into two sub-periods according to the time-space collocation between the fault mesh and hydrocarbon generation, the section 5.2 we discussed.

### **The first stage (Permian to Triassic)**

The hydrocarbon originated from an O source rock in the southern study area of the Manjiaer Depression, migrated along a hydrocarbon source network to the Donghe sandstone traps, and accumulated. The Donghe sandstone in the north was uplifted to the surface during intensive compressive deformation in the Permian to the Triassic (Fig. 13g, h) and was directly connected with fresh water. Thus, the reservoir formation period was simultaneous with hydrocarbon accumulation and experienced water washing and biodegradation. The bitumen formed near the unconformity interface and partial reservoir at the base of the Donghe sandstone reservoirs underwent long-term biodegradation (Fig. 13d), and bitumen exists in well DH13 (Table 1), located in the saddle.



There was strong volcanic activity during the Permian to the Triassic, we suggest that the high contents of CO<sub>2</sub> and N<sub>2</sub> in the Donghe sandstone reservoir was due to volcanic degassing.

The second stage (Jurassic to Cretaceous)

This stage can be divided into two sub-stages based on the hydrocarbon generation periods. In the first sub-stage, during J<sub>1-2</sub> before hydrocarbon generation, the hydrocarbon reservoirs that accumulated in the transient storage of the Donghe sandstone during the Permian to the Triassic migrated by a fully-connected hydrocarbon source network along fault F5 to the Jurassic traps. The second sub-stage was the hydrocarbon generation period during the J<sub>3</sub> to Cretaceous. The hydrocarbon migrated by a transient storage-unconformity relay style and fault-unconformity relay style to the Donghe sandstone transient storage traps, J<sub>IV</sub> braided river deposits transient storage traps, and J<sub>III</sub> alluvial fan petroleum accumulation network and accumulated (Fig. 13c). The Jurassic strata were then buried to a depth shallower than 500 meters in this stage (Fig. 13f), a depth conducive to biodegradation. The heavy oil from the Jurassic reservoirs formed in this stage.

The third stage (Eocene)

The thrust faults in the Paleozoic were reactivated during inversion. The hydrocarbon generated in this stage migrated by a fully-connected hydrocarbon source rocks style, fault-transient storage-unconformity relay style and fault-unconformity-transient storage relay style to the traps in the transient storage of the Donghe sandstone, and J<sub>IV</sub> braided river deposits and petroleum accumulation network of the J<sub>III</sub> alluvial fan deposits and accumulated to form a reservoir (Fig. 13b). The normal oil in the Jurassic reservoirs was accumulated in this stage.

The fourth stage (Miocene)

The gaseous hydrocarbon charged in this stage originated from oil and kerogen cracking. Gas washing occurred in the earlier hydrocarbon reservoirs during gaseous hydrocarbon charging. The crude oil was dissolved and the light hydrocarbon fraction migrated to the traps by faults and the unconformity and formed condensate and light hydrocarbon (Silverman, 1985; Thompson, 1987, 1988; Masterson et al., 2001; Meulbroek et al., 1998). There is evidence of condensate reservoirs formed by gas washing in the Ordovician and Carboniferous reservoirs in the Tazhong and Tabei Uplift, Tarim Basin (Zhu et al., 2013; Chen et al., 2014). The gaseous hydrocarbon originated from the same source rock in the Donghe sandstone and the Jurassic reservoirs, which indicates that the gaseous hydrocarbon in the Jurassic reservoirs must have migrated through the lower part of the Donghe sandstone reservoirs and in that process the Donghe sandstone reservoirs experienced gas washing. The light hydrocarbon fraction was formed by gas washing when it migrated along faults and the unconformity to the Jurassic traps and accumulation to form condensate reservoirs (Fig. 13a).

There are multiple periods of hydrocarbon accumulation and adjustment, and hydrocarbons migrated and accumulated by a fault mesh style to the clastic rock reservoirs in the study area. The transient storage of the Carboniferous Donghe sandstone was connected with the transient storage of the J<sub>IV</sub> formation in different fault mesh types (Fig. 11). The hydrocarbon that originated from the Ordovician source rocks of the southern Manjiaer Depression temporarily accumulated in the transient storage of the Donghe sandstone during the Permian to the Triassic. The hydrocarbon that accumulated in the transient storage of the Donghe sandstone experienced gas washing and formed a light hydrocarbon fraction during the Jurassic to the Miocene. These hydrocarbons migrated along a fault mesh and adjusted to the Jurassic transient storage and petroleum accumulation network and accumulated in the Jurassic traps, forming secondary condensate reservoirs in the Jurassic.

## **5.5 The hydrocarbon exploration significance of the fault mesh petroleum plays in the study area**

There are two different sedimentary origins of the transient storage units in the study area, which

determined the different exploration targets in the Carboniferous Donghe sandstone and the Jurassic. The main target in the shoreline deposits of the Donghe sandstone is fault-related reservoirs because of the lack of mudstone. Faults are a three-dimensional geological body with complex architecture (Chester et al., 1993; Caine et al., 1996; Childs et al., 1997; Aydin, 2000; Yielding et al., 2000), and the faults with sandstone self-juxtaposition can seal laterally through fault rocks and deformation bands (Fossen et al., 2007, 2011; Faulkner et al., 2010; Tueckmantel et al., 2010). We suggest that deformation band clusters seal some faults in the study area, following an integrated analysis of the original formation fluids and faulting mechanisms, and formed fault-block reservoirs (Fig. 14a). The discussion of sandstone self-juxtaposition faults closure is beyond the scope of this study and is not discussed here. The lava-shielded reservoirs may exist in the transient storage of the Donghe sandstone because of volcanic activity during the Permian to the Triassic (Fig. 14b).

The exploration target related to the inner-transient storage and upper-transient storage can be found in the Jurassic. For the  $J_{IV}$  braided river deposits of transient storage, the channelized lithologic related reservoirs (Fig. 14c) and sandbank lenses stratigraphic related reservoirs (Fig. 14d) are present due to the migration of channels, and fault-block reservoirs related to the channel sandstone and faults (Fig. 14e). The  $J_{III}$  formation is an alluvial fan depositional system as a petroleum accumulation network, the related of upper-transient storage reservoirs can be found with composition of  $J_{IV}$  braided river deposits, such as stratigraphic related reservoirs for the fast change of rock facies (Fig. 14f).

## 6 Conclusions

(1) There are four periods of hydrocarbon charging, with oil charging during the first three periods and gas charging during the last. These periods are characteristic of reservoir formation with fault mesh migration and accumulation in the clastic rock reservoirs in the Donghetang area, Tabei Uplift, Tarim Basin, NW China. The hydrocarbon accumulation process of fault mesh petroleum plays is the key reason that there are multi-strata reservoirs in the study area, but each has different hydrocarbon properties.

(2) There are two sets of fault meshes in the study area: the Donghe sandstone and Permian and Triassic strata combination as well as the  $J_{IV}$  and  $J_{III}$  formation combination in the Jurassic strata.

(3) The hydrocarbon of the Donghe sandstone and Jurassic reservoirs originate from the same source rocks, marine hydrocarbon from the southern Manjiaer Depression. The reservoirs of the Jurassic have a light hydrocarbon fraction that originated from gas washing of the Donghe sandstone reservoirs and migrated by a different carrier system style to the Jurassic traps and formed secondary condensate reservoirs.

(4) The reservoirs in the Donghetang area are typical allochthonous and far source fault mesh petroleum plays. The highly effective hydrocarbon carrier system is key for hydrocarbon accumulation.

(5) The hydrocarbon carrier system in the fault mesh petroleum plays in the study area can be divided into fully-connected, fault-unconformity-transient storage relay, fault-transient storage-unconformity relay, and transient storage-fault relay styles according to the architecture of the fault mesh. The different compositions of the fault mesh units can form three categories, including upper-transient storage, inner-transient storage and margin-transient storage reservoirs, as well as 15 types of reservoirs.

## Acknowledgment

The authors are thankful for permission to publish this paper and acknowledgment for data contribution and sample collection from the Research Institute of Petroleum Exploration and Development in Tarim Oilfield Company, PetroChina. This research was funded by the National Science and Technology Major Project (NO. 2017ZX05001) in China. We are grateful to editors and anonymous reviewers for very constructive and useful

comments.

## References

- Aydin A., 2000. Fracture, faults, and hydrocarbon entrapment migration and flow. *Marine and Petroleum Geology*, 7 (17): 797–814.
- Caine J. S., Evans J.P, and Forster C.B, 1996, Fault zone architecture and permeability structure: *Geology*, 24: 1025–1028.
- Chang X.C., Wang T.G., Li Q.M., Cheng B., Zhang L.P., 2013. Geochemistry and possible origin of petroleum in Palaeozoic reservoirs from Halahtang Depression. *Journal of Asian Earth Sciences*, 47: 129–141.
- Cheng B., Wang T.G., Chen Z.H., Chang X.C., Yang F.L., 2016. Biodegradation and possible source of Silurian and Carboniferous reservoir bitumens from Halahatang sub-depression, Tarim Basin, NW China. *Marine and Petroleum Geology*. 78:236–246.
- Chester F. M., Evans J.P., and Biegel R.L., 1993. Internal structure and weakening mechanisms of the San Andreas fault: *Journal of Geophysical Research-Solid Earth*, 98 (1): 771–786.
- Childs C., Watterson J., and Walsh J. J., 1996. A model for the structure and development of fault zones: *Journal of the Geological Society (London)*, 153: 337–340.
- Dow W.G., 1972. Application of oil correlation and source rock data to exploration in Williston Basin (abs.). *AAPG Bulletin*, 56:615.
- Dow W.G., 1974. Application of oil correlation and source rock data to exploration in Williston Basin. *AAPG Bulletin*, 58 (7): 1253–1256.
- Demaison G., 1984. The generative basin concept. In: *Petroleum Geochemistry and Basin Evaluation* (ed. by G. Demaison and R.J. Murris). American Association of Petroleum Geologists Memoir, 35, 1–14.
- Faulkner D.R., Jackson C.A.L., Lunn R.J., Schlische R.W., Shipton Z.K., Wibberley C.A.J., Withjack M.O., 2010. A review of recent developments concerning the structure, mechanics and fluid flow properties of fault zones. *J. Struct. Geol.* 32(11), 1557–1575.
- Fossen H., Bale A., 2007. Deformation bands and their influence on fluid flow. *AAPG Bull.* 91 (12), 1685–1700.
- Fossen H., Schultz R.A., Shipton Z.K., Mair K., 2007. Deformation bands in sandstone: a review. *J. Geol. Soc.* 164 (4): 755–769.
- Fossen H., Schultz R.A., Torabi A., 2011. Conditions and implications for compaction band formation in the Navajo Sandstone, Utah. *J. Struct. Geol.* 33 (10): 1477–1490.
- Hooper E. C. D., 1991 . Fluid migration along growth fault in compacting sediments . *Journal of Petroleum Geology*, 14:161—180.
- Hu C.Y., 1986. An approach on regional controlling factors of oil-gas field distribution in offshore sedimentary basins of China (in Chinese with English abstract). *Marine Geology & Quaternary Geology*, 6(4): 23–29.
- Huang H.P., Zhang S.C., Su J, 2016. Palaeozoic oil-source correlation in the Tarim Basin, NW China: A review. *Organic Geochemistry*, 94: 32–36.
- Indrevær K., Stunitz H., Bergh S.G., 2014. On Palaeozoic–Mesozoic brittle normal faults along the SW Barents Sea margin: fault processes and implications for basement permeability and margin evolution. *J. Geol. Soc.* 171 (6), 831–846.
- Jin Z.J., Wang Q.C., 2004. New progresses in research of China,s typical superimposed basins and reservoiring of hydrocarbons: taking Tarim basin as an example [J]. *Science in China Series (D-Earth Sciences)*, 34(Suppl I): 1–12. (in Chinese).

- Knipe R.J., 1997. Juxtaposition and seal diagrams to help analyze fault seals in hydrocarbon reservoirs. *Am. Assoc. Pet. Geol. Bull.* 81 (2), 187–195.
- Lei, Z. C., Xu, H. M., Jiang, T. W., Li, Z. C., Li, J. W., Li, W. L., Xiong, Y. B., Li, S. Z., Zhao, J. W., 2019. Multiple phase hydrocarbons from Carboniferous reservoir rocks and their origin in the Donghetang area, Western Tabei Uplift, Tarim Basin, NW China. *Russian Geology and Geophysics*, 60(2), 215-230.
- Li D.S., Liang D.G., Jia C.Z., Wang G., Wu Q.Z., He D.F., 1996. Hydrocarbon accumulation in the Tarim Basin, China. *AAPG Bulletin*, 80(10): 1587-1603.
- Li W.L., Xu H.M., Niu Y.J., Wang C., Gao S.Y., 2016. Sand body types of clastic shore deposits with delta backgrounds and their control over reservoir quality. *Arab J Geosci*, 9:247.
- Liang D.G., Gu Q.Y., Pi X.J., 1998. Distribution law of the condensate gas reservoir in Tabei Uplift (in Chinese with English abstract). *Natur. Gas Ind.*, 18 (3):5-9.
- Liu Y.L., Huang Z.B., Wu G.Y., Wu G.Y., Zhen D.M., 2012.  $^{40}\text{Ar}$ - $^{39}\text{Ar}$  geochronology and geochemistry of the volcanic rocks from the west segment of Tabei Uplift, Tarim Basin (in Chinese with English abstract). *Acta Petrologica Sinica*, 28 (8): 2423-2434.
- Mango F.D., 1987. An invariance in the isoheptanes of petroleum. *Science* 273, 514-517.
- Mango F.D., 1990b. The origin of light cycloalkanes in petroleum. *Geochim.Cosmochim.Acta* 54, 23-27.
- Maggoon L.B., 1988. The petroleum system: A classification scheme for research, exploration and resources assessment, in L.B.Maggon, ed., *Petroleum systems of the United States*. USGS Bulletin, 1870: 2-15.
- Maggoon L.B., 1992. Identified petroleum systems within the United States-1992, in L.B.Maggon, ed., *The petroleum system status of research and methods*, 1992. USGS Bulletin, 2007: 2-11.
- Magoon L.B. and Dow W.G., 1994. The petroleum system: From source to trap. *AAPG Memoir* 60, 3-24.
- Mastern W.D., Dzou L.I.P., Holba A.G., Fincannon A.L., Willis L., Dzou L.I.P., 2001. Evidence for biodegradation and evaporative fractionation in West Sak, Kuparuk and Prudhoe Bay field areas, North Slope, Alaska. *Organic Geochemistry*, 32 (3): 411-411.
- Meissner F.F., 1984. Petroleum geology of the Bakken Formation, Williston basin, North Dakota and Montana, in G.Demaison and R.J.Murris, eds., *Petroleum geochemistry and basin evaluation*. AAPG Memoir 35, 159-179.
- Meulbroek P., Cathles L., Whelan J., 1998. Phase fractionation at South Eugene Island Block 330. *Organic Geochemistry*, 29 (1): 223-239.
- Pang X.Q., Jin Z.J., Jiang Z.X., Zuo S.J., 2003. Evaluation of hydrocarbon resources of superimposed basin and its significance (in Chinese with English abstract). *Petroleum Exploration and Development*, 29 (1): 9-13.
- Pang X.Q., Zhou X.Y., Lin C.S., Huo Z.P., Luo X.R., Pang H., 2010. Classification of complex reservoirs in superimposed basins of western China. *Acta Geological Sinica*, 84(5): 1011-1034.
- Perrodom A., 1983a. Dynamics of oil and gas accumulation. *Pau. Elf Aquitaine*, 187-210.
- Perrodom A., 1992. Petroleum systems: models and applications. *Journal of Petroleum Geology*, 15 (3): 319-326.
- Randi S. Martinsen, 2003a. Depositional remnants, part1: Common components of the stratigraphic record with important implication for hydrocarbon exploration and production. *AAPG Bulletin*, 87 (12): 1869-1882.
- Randi S. Martinsen, 2003b. Depositional remnants, part2: Examples from the Western Interior Cretaceous basin of North America. *AAPG Bulletin*, 87 (12): 1869-1882.
- Silverman S.R., 1985. Migration and segregation of oil and gas. *AAPG Bulletin, Mem.*, 4: 53-65.
- Tang L.J., Qi L.X., Qiu H.J., Yun L., Li M., 2012. Poly-phase differential fault movement and hydrocarbon accumulation of the Tarim Basin, NW China (in Chinese with English abstract). *Acta Petrologica Sinica*, 28(8): 2569-2583.
- Tang L.J., Jin Z.J., Zhang Y.W., Lu K.Z., 1999. Negative inversion structures and geological significance of northern Uplift, the Tarim Basin, NW China (in Chinese with English abstract). *Geoscience*, 13(1): 93-98.

- Thompson K.F.M., 1987. Fractionated aromatic petroleum and the generation of gas-condensates. *Org. Geochem.*, 11(6): 573-590.
- Thompson K.F.M., 1988. Gas-condensate migration and the petroleum fractionation in deltaic systems, *Marine Petroleum Geology*, 5(4): 237-245.
- Tueckmantel, C., Fisher, Q.J., Knipe, R.J., Lickorish, H., Khalil, S.M., 2010. Fault seal prediction of seismic-scale normal faults in porous sandstone: a case study from the eastern Gulf of Suez rift, Egypt. *Mar. Pet. Geol.* 27(2): 334-350.
- Ulmishek G., 1986. Stratigraphic aspects of petroleum resource assessment, in D.D.Rice, ed., *Oil and gas assessment methods and application*. AAPG Studies in Geology, 21 :59-68.
- Wang F.Y., He P., Zhang S.C., Zhao M.J., Lei J.J., 1997. The K-Ar isotopic dating of authigenic illites and timing of hydrocarbon fluid emplacement in sandstone reservoir (in Chinese with English abstract). *Geological Review*. 43 (5): 540-546.
- Wang Y.P., Zhao C.Y., Wang Z.Y., Wang H.H., Tian J., Zou Y.R., Liu Z.Z., 2008. Identification of marine natural gases with different origin sources. *Sci. China (Ser. D)*, 51 (Suppl. 1): 148-164.
- Wang Y.S., Li M.W., Pang X.Q., Zhang S.W., Shi D.S., Dong X., 2005. Fault-fracture mesh petroleum plays in the Zhanhua Depression, Bohai Bay Basin: Part 1. Source rock characterization and quantitative assessment. *Organic Geochemistry*, 36: 183-302.
- Wang Z.M., Tian J., Shen Y.M., Zhou L.X., Wang Z.Y., 2004. Sedimentary facies of Donghe Sandstone during the late Devonian to Early Carboniferous in Tarim Basin (in Chinese with English abstract). *Journal of Palaeogeography*, 6 (3): 289-295.
- Wu K.Y., Li L.L., Zha M., 2009. Vertical structures of unconformity and its simulation experiment of hydrocarbon accumulation mechanism (in Chinese with English abstract). *Petroleum Geology and Experiment*, 31(5): 537-541.
- Xu H.M., Xu Z.H., Zhang S.W., Wang Z.G., Wang Y.S., 2008. Layer structure petroleum accumulation system and characteristic of subtle reservoir of continental basin in eastern China: Taking Jiyang Depression for example (in Chinese with English abstract). *Science in China (Series D)*, 38 (S1): 129-137.
- Yielding G., Bretan P., and Freeman B., 2010, Fault seal calibration: A brief review, in Jolley, S.J., Fisher, Q.J., Ainsworth, R.B., Vrolijk, P.J., and Delisle, S., eds., *Reservoir Compartmentalization: Geological Society of London Special Publication 347*, p. 243-255, doi:10.1144/SP347.14.
- Zhang B., Zhu G.Y., Su J., Lu Y.H., 2012. Origin and distribution of hydrocarbon in Donghe Oilfield, west Tabei Uplift, Tarim Basin (in Chinese with English abstract). *Earth Science Frontier*, 19(4): 276-283.
- Zhang S.C., Zhang B., Yang H.J., et al., 2012. Adjustment and alteration of hydrocarbon reservoirs during the late Himalayan period, Tarim basin, NW China. *Petroleum Exploration and Development*, 9(6), 668-680.
- Zhang S.C., Hanson D.G., Liang D.G., Chang E., Fago F., Hanson A.D., 2000. Paleozoic oil source rock correlation in the Tarim Basin, NW China. *Organic Geochemistry*, 31 (4):273-286.
- Zhang S.C., Liang D.G., Li M.W., Xiao Z.Y., He Z.H., 2002. Molecular fossils and oil-source rock correlations in the Tarim Basin, NW China. *Chinese Science Bulletin* , 47 (Suppl. ): 20-27.
- Zhang S.W., Lin H.X., Shen Y., 2013. Analysis on meshwork-carpet pool-forming mechanism of Chepaizi Uplift and enlightenment on petroleum exploration of Junggar Basin (in Chinese with English abstract). *Geological Review*, 59(3): 489-500.
- Zhang S.W., Wang Y.S., Shi D.S., Xu H.M., 2003. Fault-fracture mesh petroleum play: An Example from the Neogene of the Jiyang Superdepression (in Chinese with English abstract). *Petroleum Exploration and Development*, 30 (1): 1-10.
- Zhang S.W., Wang Y.S., Shi D.S., Xu H.M., Pang X.Q., Li M.W., 2004. Fault-fracture mesh petroleum plays in the

- Jiyang Superdepression of the Bohai Bay Basin, eastern China. *Marine and Petroleum Geology*, 21: 651-668.
- Zhang Y.M., Wang B., Ou G.X., 2006. Research on Jurassic oil-gas accumulated period and order in Kongquehe region, Tarim Basin (in Chinese with English abstract). *Petroleum Geology and Engineering*, 20(5): 2-5.
- Zhang Y.Y., Luo X.Q., 2012. K-Ar and Ar-Ar dating of authigenic illite and hydrocarbon accumulation history of carboniferous and Silurian sandstone reservoirs in well Ha 6, Tarim basin (in Chinese with English abstract). *Acta Petroleum Sinica*, 33(5): 748-755.
- Zhao W.Z., He D.F., 2000. Concept and its significance of composite petroleum systems in China (in Chinese with English abstract). *Petroleum Explorations*, 5(3):1-12.
- Zhu G.Y., Zhang S.C., Su J., 2013. Secondary accumulation of hydrocarbons in Carboniferous reservoirs in the northern Tarim Basin, China. *Journal of Petroleum Science and Engineering*. 102:10-26.
- Zhu G.Y., Zhang S.C., Su J., Zhang B., Yang H.J., Zhu Y.F., Gu L.J., 2013. Alteration and multi-stage accumulation of oil and gas in the Ordovician of the Tabei Uplift, Tarim Basin, NW China: Implications for genetic origin of the diverse hydrocarbons. *Marine and Petroleum Geology*, 46: 234-250.

## Figures

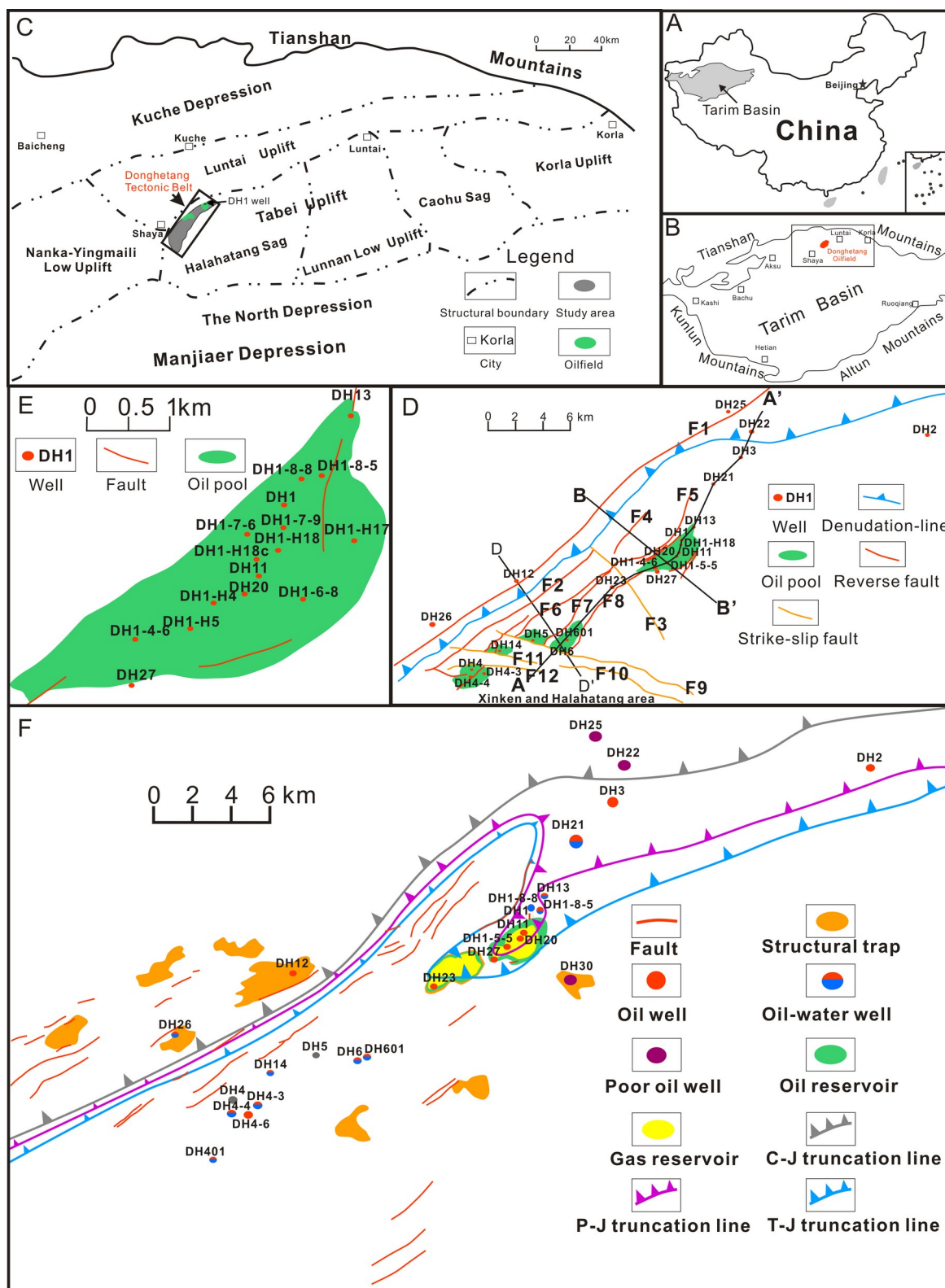


Fig. 1. A, B, C are the structural locations of Tarim Basin, Tabei Uplift and Donghetang tectonic belt, respectively, and D is the fault system in the Carboniferous Donghe sandstone. E is the well location in the DH1 Oilfield, and F is

the fault system in the Jurassic.

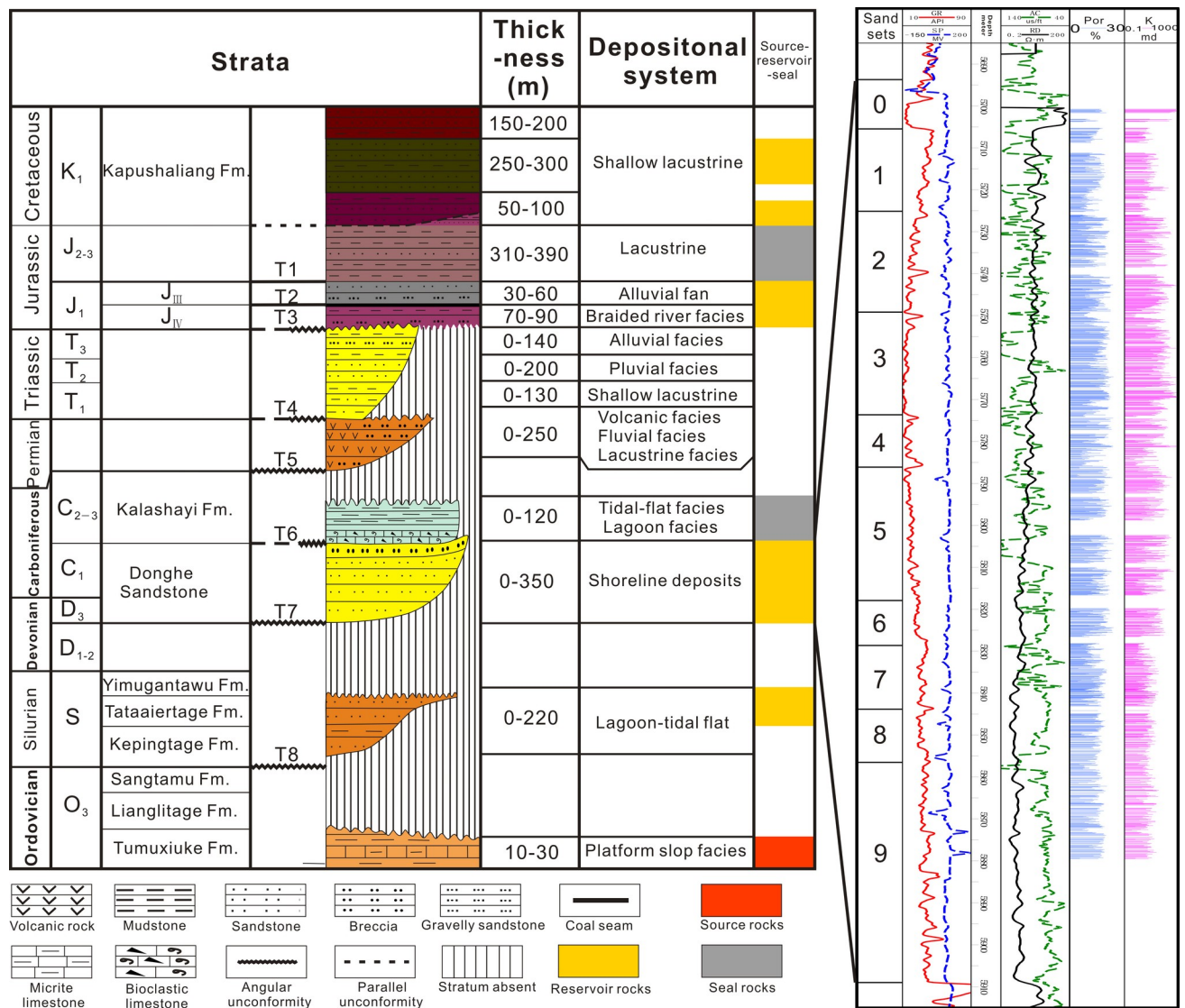


Fig. 2. The geological column map in the Donghetang area. The petrophysical properties in the DH11 well core section of the Carboniferous Donghe sandstone from the well core data.



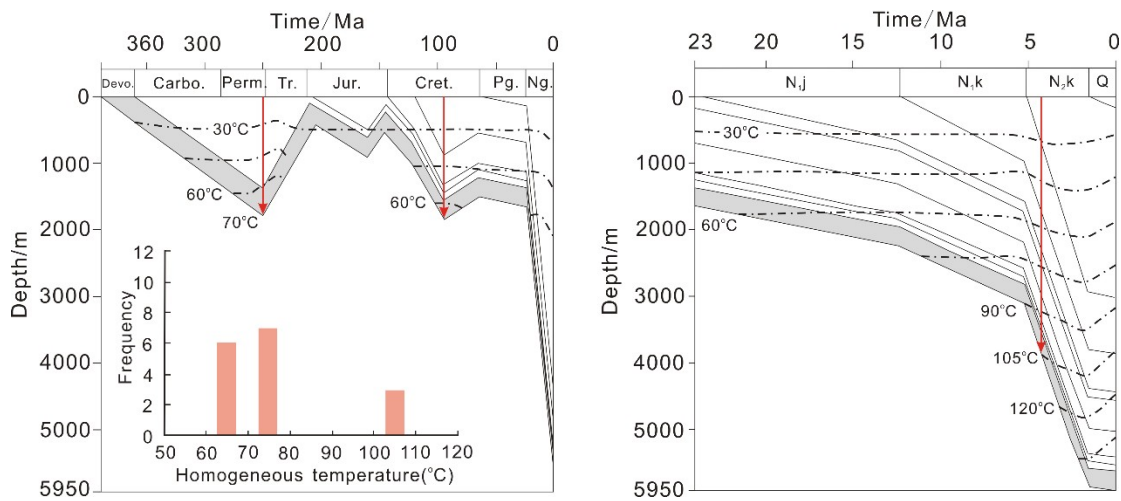


Fig.3. The depth-thermal history and hydrocarbon charging periods of the Donghe sandstones reservoir, DH1 oilfield, and the rectangle filling with grey marks the Donghe sandstones. The histogram of homogeneous temperature of salted-water inclusions associated with hydrocarbon inclusion in the well DH11 is after Zhang et al., (2012). The Neogene of hydrocarbon charging is after Zhang and Luo (2012) who used the K-Ar dating of authigenic illite of Carboniferous sandstone reservoirs in the well Ha6 from the Halahatang sag.

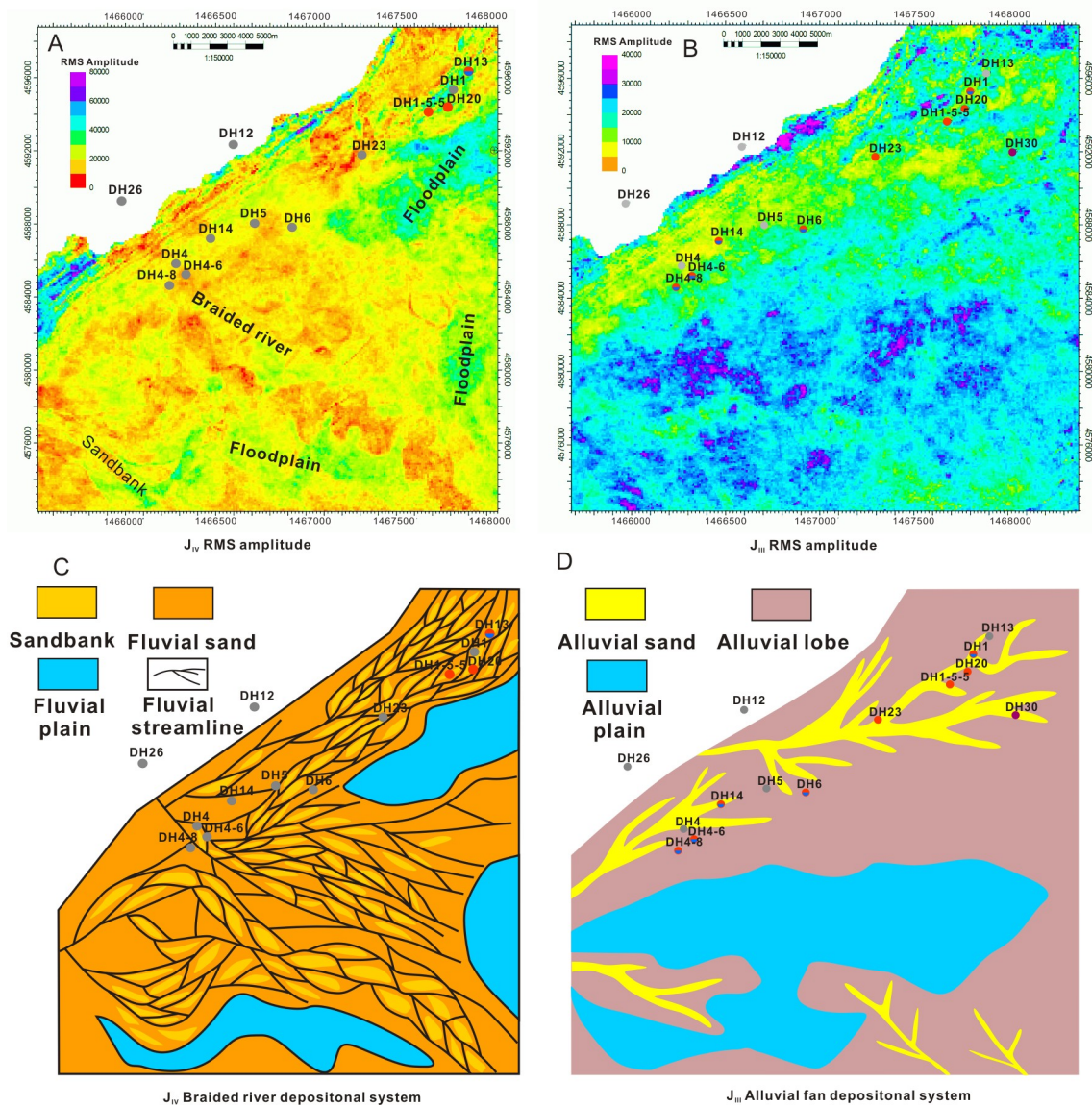


Fig. 4. The RMS amplitude of the  $J_{IV}$  formation and  $J_{III}$  formation and its interpretation. Partial hydrocarbons are in wells distributed in the  $J_{IV}$  and the  $J_{III}$  formations. The legend of the hydrocarbon well is shown in Fig. 1F.

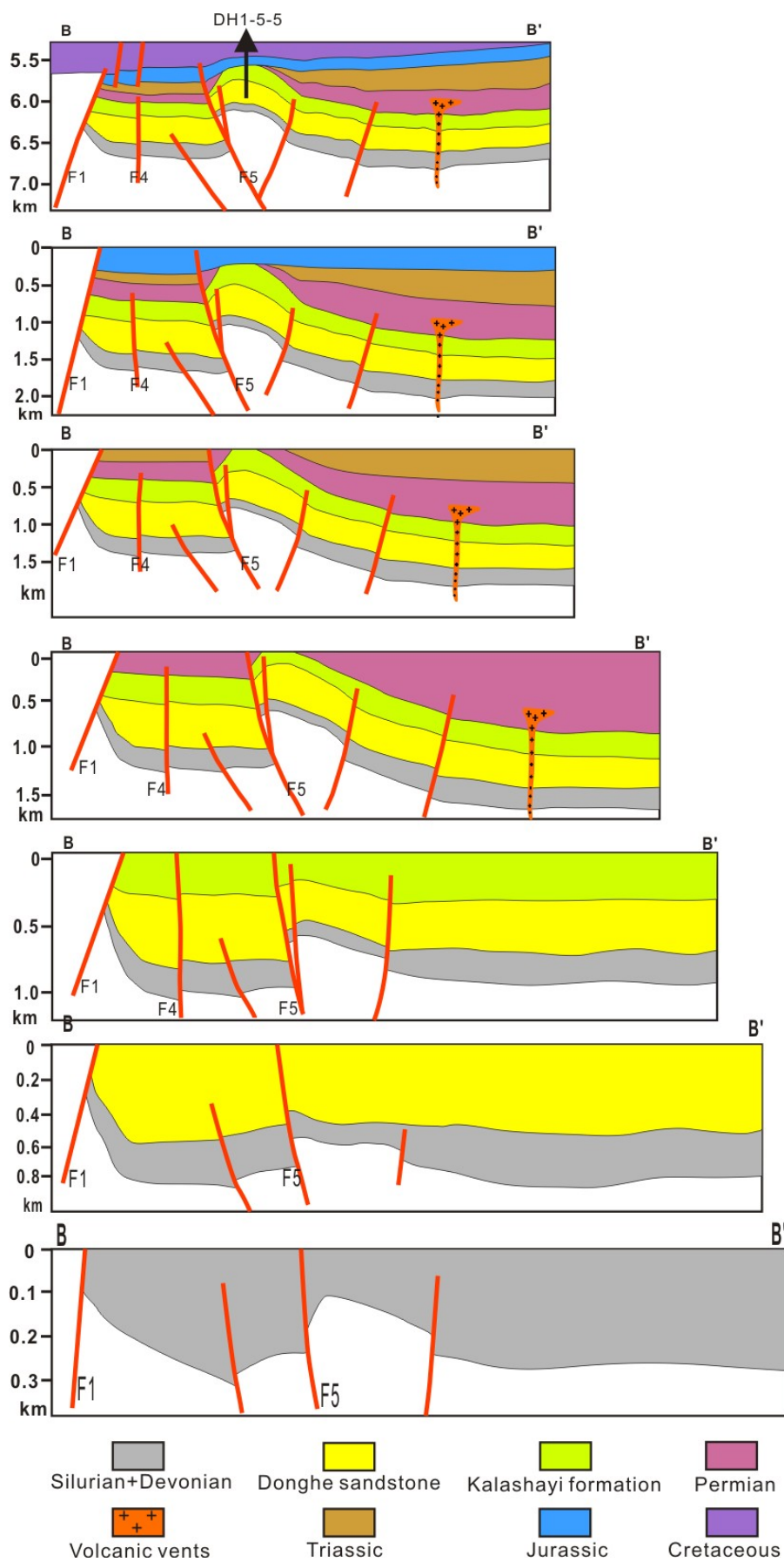


Fig. 5. The structural evolution of the Line B-B'. The profile location and fault numbers are shown in Fig. 1D.

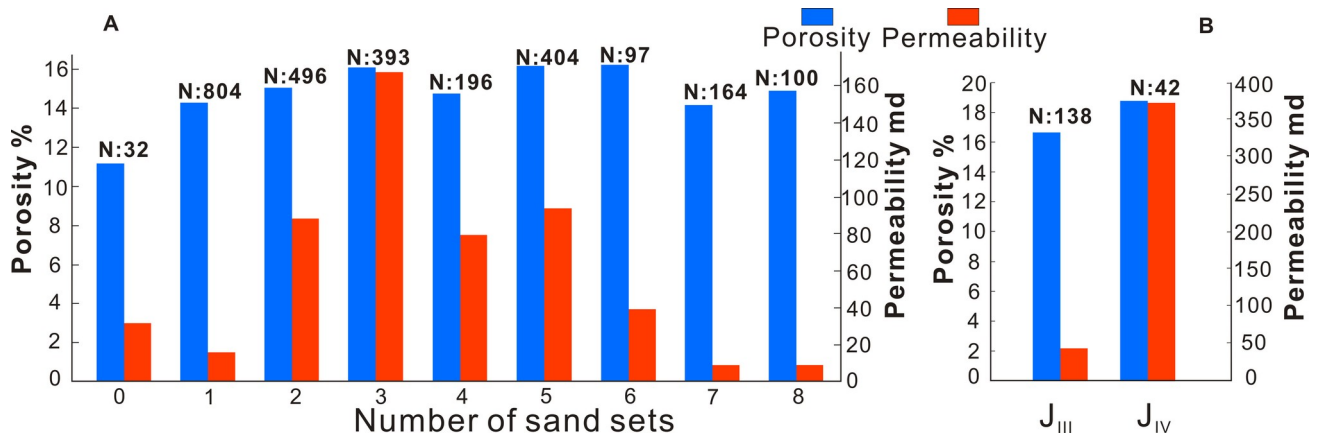


Fig. 6. The petrophysical properties of the transient storage and the petroleum accumulation network. A is the average petrophysical properties in the different sand sets of the Donghe sandstone, and B is the average petrophysical properties in the J<sub>IV</sub> formation and the J<sub>III</sub> formation. N is the sample number.

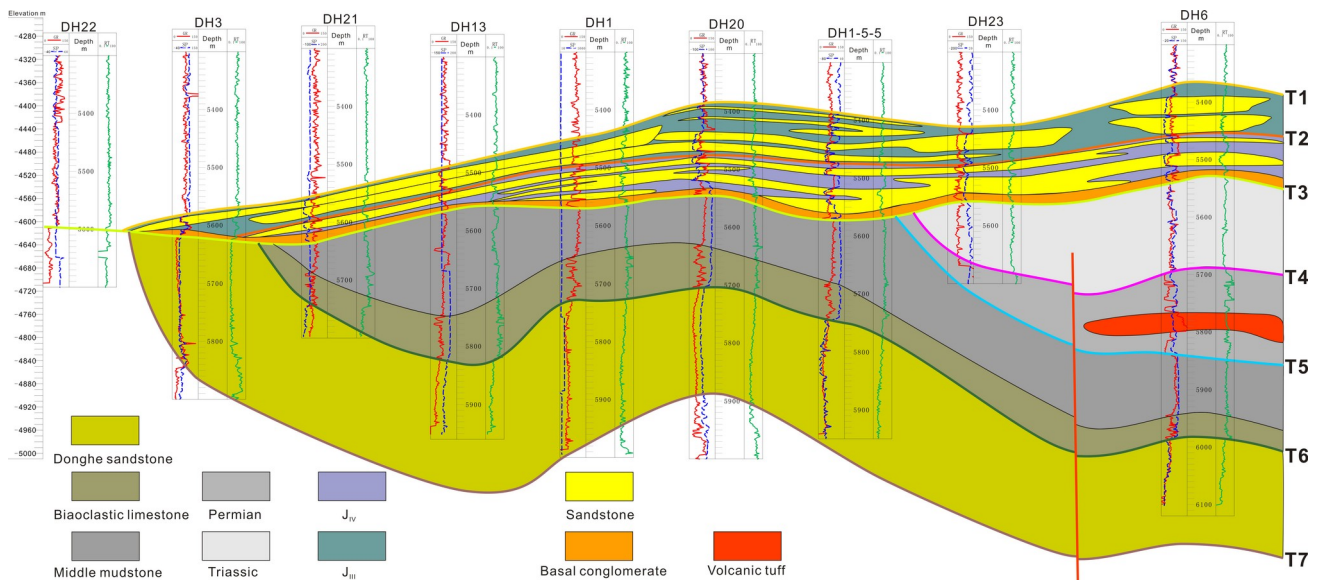


Fig. 7. The characteristics of the reservoir rock connectivity in the transient storage and the petroleum accumulation network in the study area. The transient storage of the Carboniferous Donghe sandstone is between T6 and T7, and the transient storage of the J<sub>IV</sub> formation is between T2 and T3. The petroleum accumulation network of the J<sub>III</sub> formation is between T1 and T2. There is a basal conglomerate with a thickness of 3 to 5 meters above the unconformity contact between the Jurassic and older strata. The well location is shown in Fig. 1D.



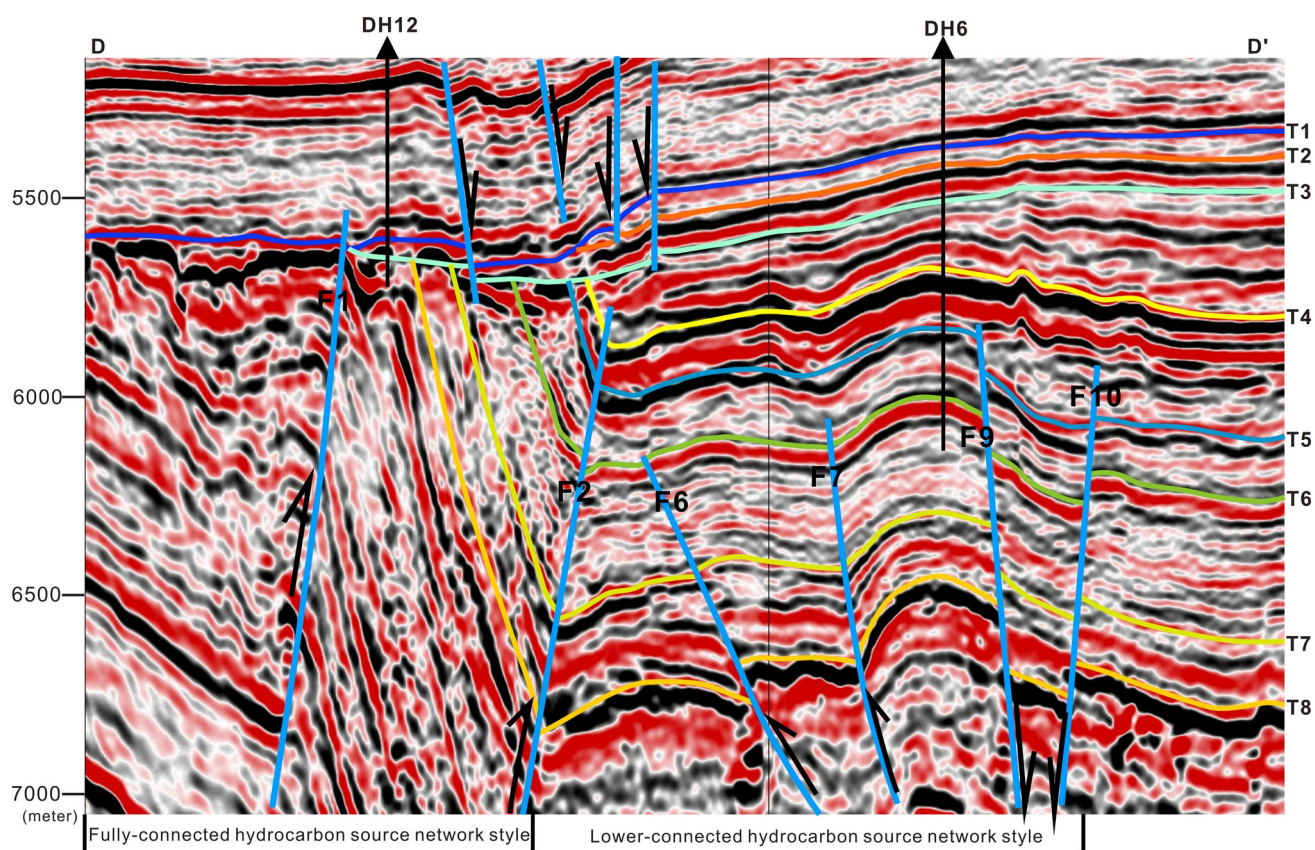


Fig. 8. The style of the hydrocarbon source network in the seismic section. The Ordovician source rocks are located below T8. The section line D-D' and well location are shown in Fig. 1D.

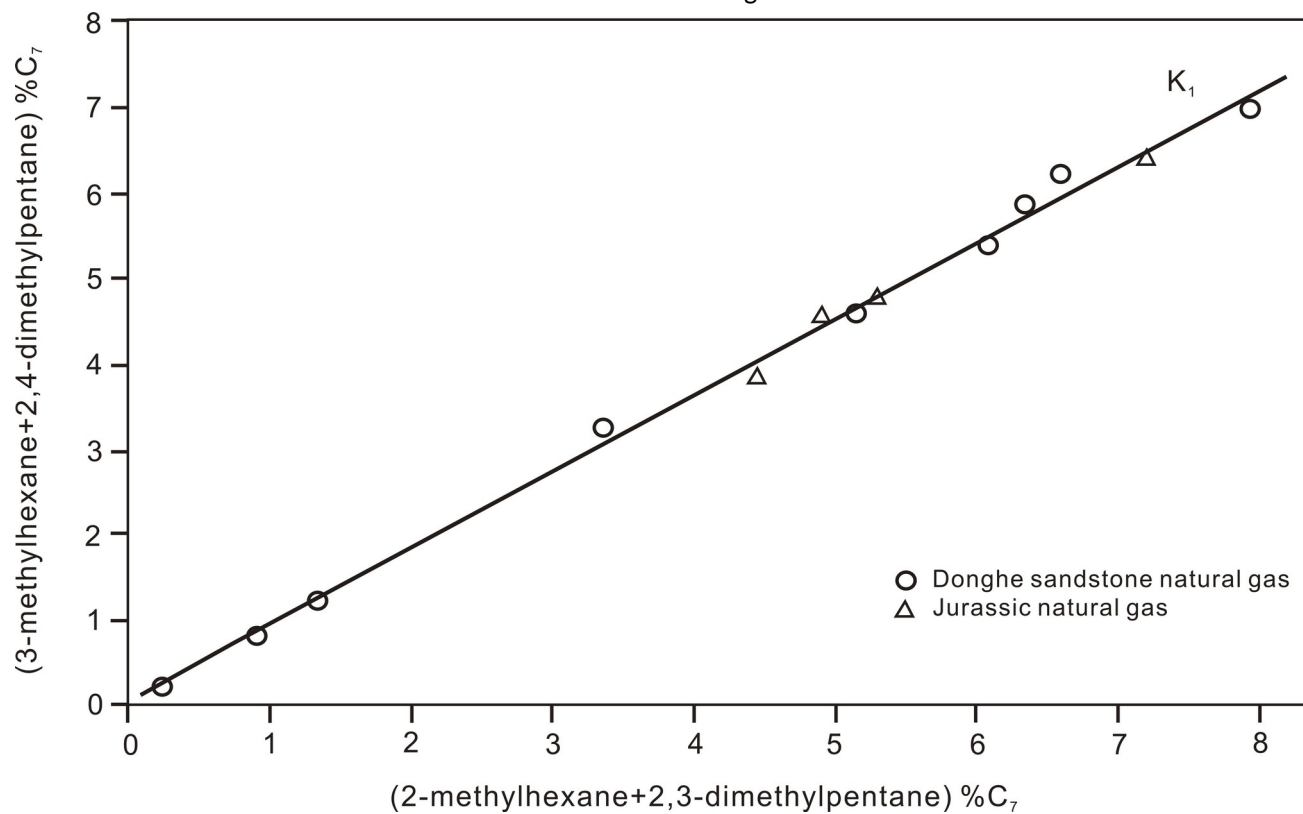


Fig. 9. Plot of (2-methylhexane+2,3-dimethylpentane) vs. (3-methylhexane+2,4-dimethylpentane).

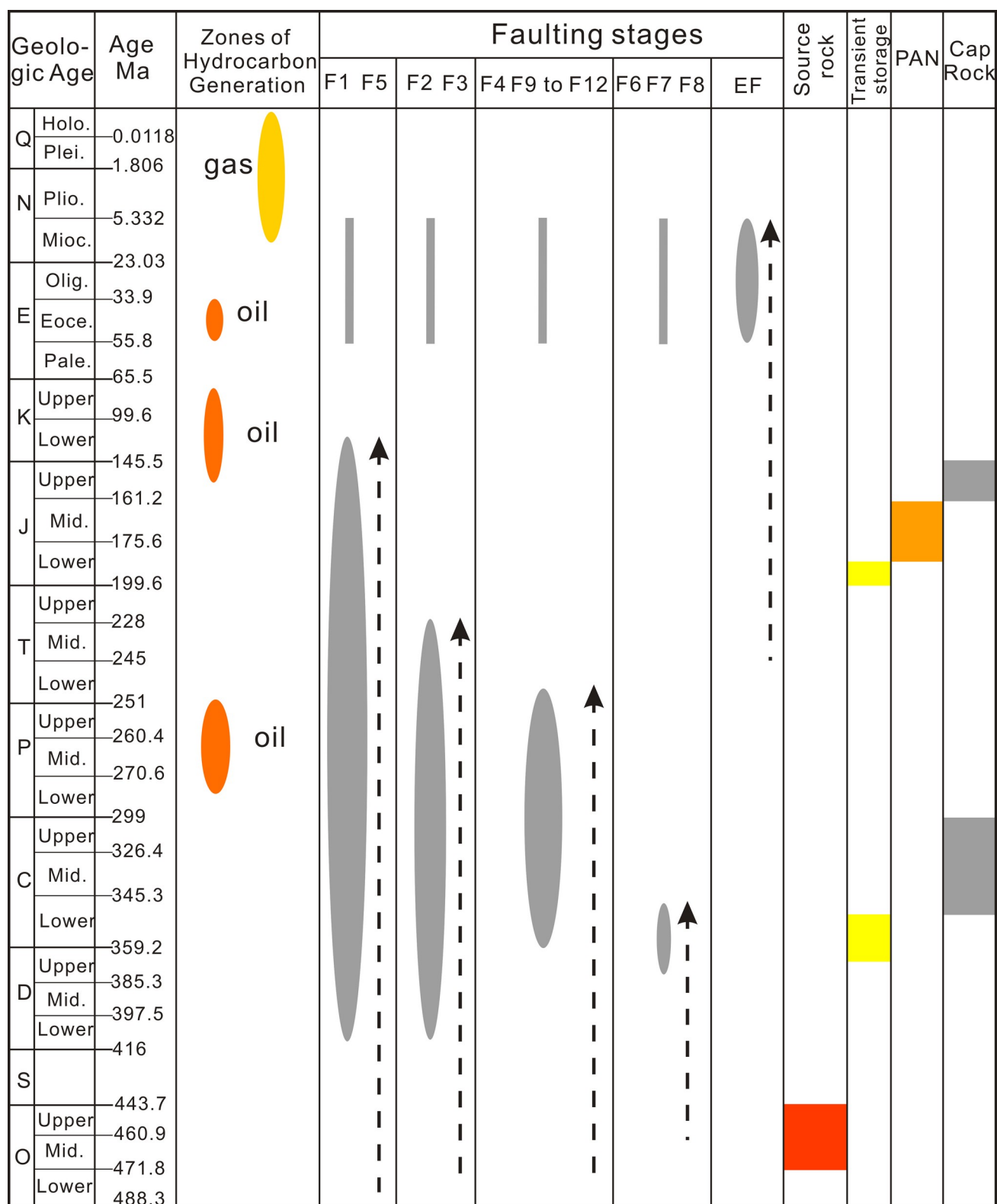


Fig. 10. The time-space collocation between the hydrocarbon generation and fault mesh. The fault numbers and locations are shown in Fig. 1D. EF, extensional faults in the Jurassic; PAN, petroleum accumulation network. The dotted line with arrows is the strata that the faults cut, the grey solid line is thrust fault that was reactivated during tectonic inversion. The ellipse is the faulting stage. Mid., Middle; Pale., Paleocene; Eoce., Eocene; Olig., Oligocene; Mioc., Miocene; Plio., Pliocene; Plei., Pleistocene; Holo., Holocene.

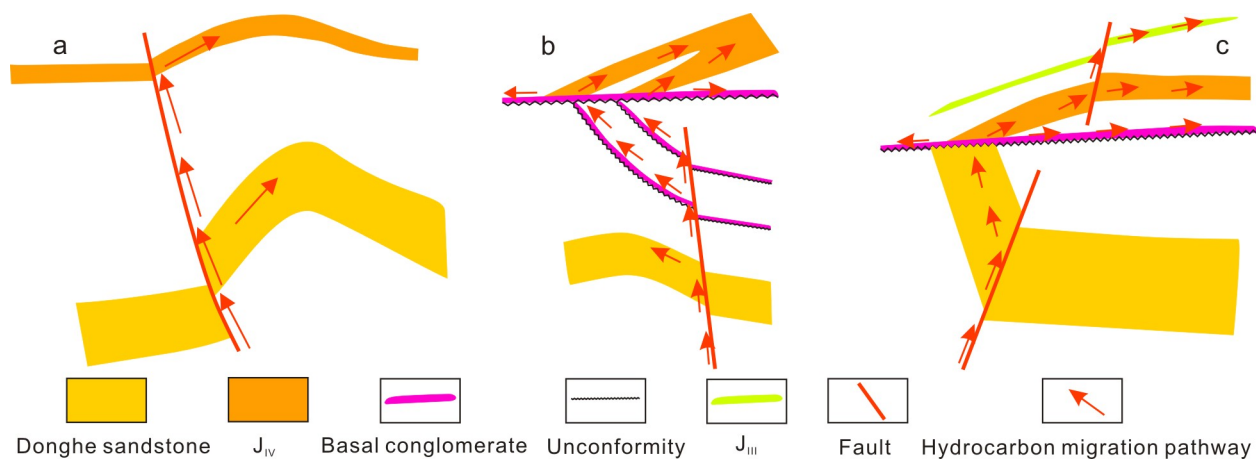
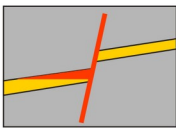
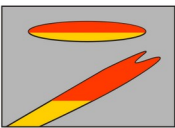
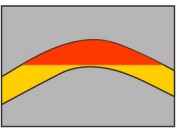
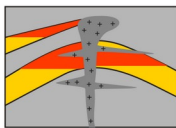
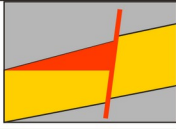
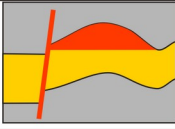
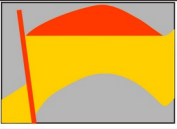
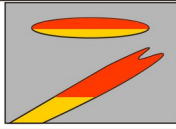
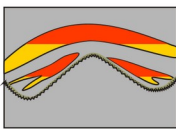
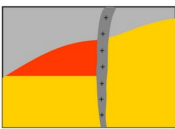
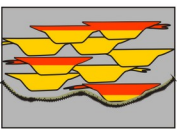
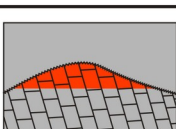

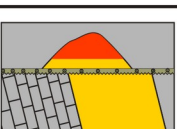
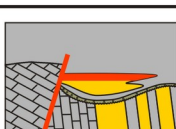

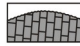


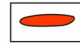
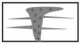
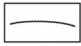




Fig. 11. The carrier system style of the fault mesh in the study area.

Upper-Transient Storage	Reservoir Model				
	Trap Type	Fault Block Traps	Lithologic Traps	Drape Anticline Traps	Lava-shielded Traps
	Potential Strata	J <sub>III</sub> J <sub>2-3</sub> K	J <sub>III</sub> J <sub>2-3</sub> K	J <sub>III</sub>	P T
	Typical Well	DH12	DH4-6	DH20	Not found yet
Inner-Transient Storage	Reservoir Model				
	Trap Type	Fault Block Traps	Fault Anticline Traps	Fault Anticline Traps	Lithologic Traps
	Potential Strata	Donghe sandstone J <sub>IV</sub>	Donghe sandstone	Donghe sandstone	J <sub>IV</sub>
	Typical Well	Not found yet	DH6	DH1	DH1-5-5
	Reservoir Model				
	Trap Type	Drape Anticline Traps	Lava-shielded Traps	CLT	
	Potential Strata	J <sub>IV</sub>	Donghe sandstone	J <sub>IV</sub>	
	Typical Well	DH20	Not found yet	Not found yet	
Margin-Transient Storage	Reservoir Model				
	Trap Type	Buried Hill Traps	Truncation Traps	Erosional Remnant	Lithologic Traps
	Potential Strata	Pre-Silurian	Donghe sandstone	J <sub>IV</sub>	J <sub>IV</sub>
	Typical Well	Not found yet	Not found yet	DH12	Not found yet

 Mudstone   
  Buried hill   
  Limestone   
  Sandstone   
  Reservoirs   
  Igneous rock   
  Unconformity   
  Basal conglomerate   
  Fault

CLT: Channelized Lithologic Traps

Fig. 12. The reservoir models in the study area.



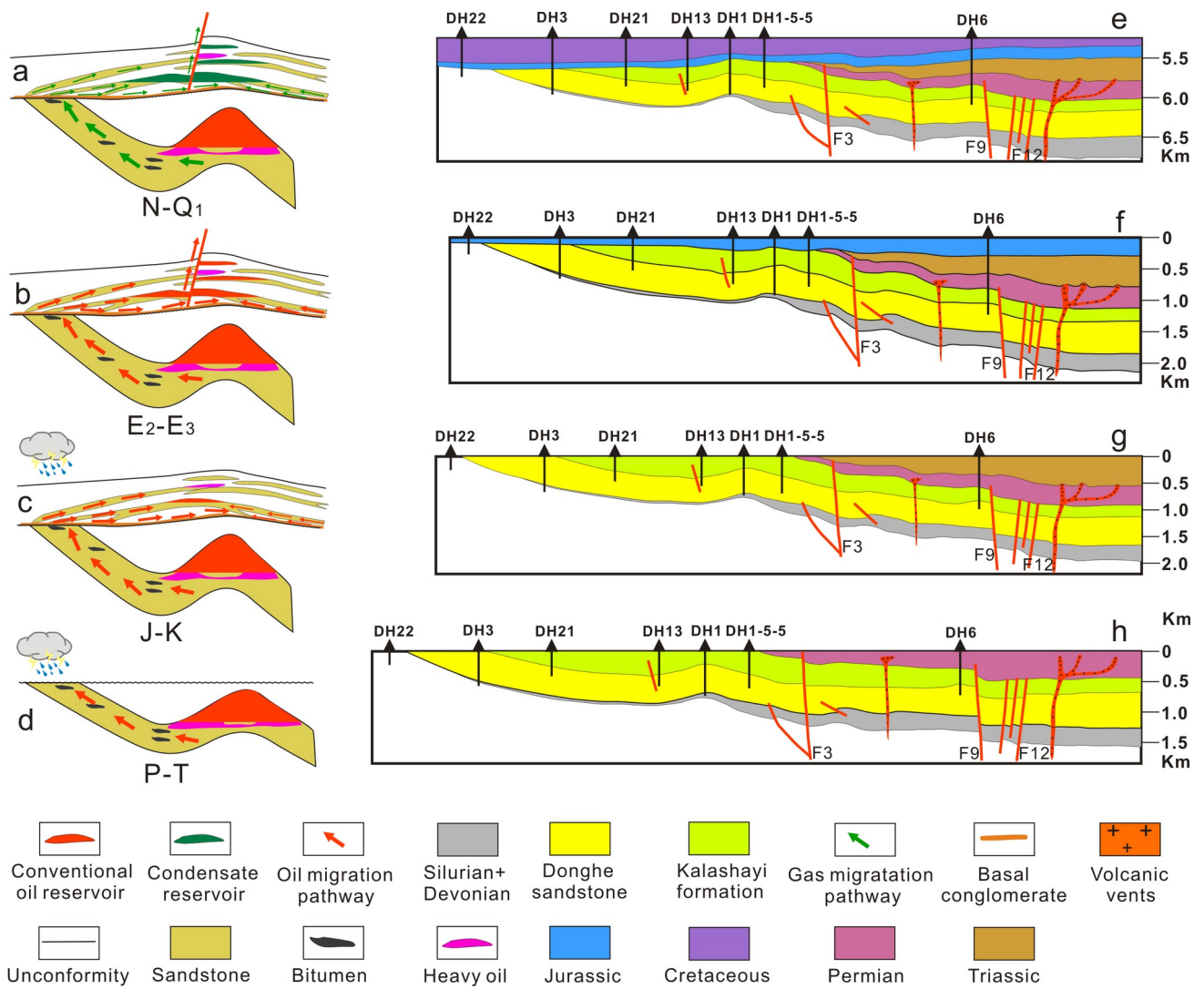


Fig. 13. The hydrocarbon accumulation process of fault mesh petroleum plays in the study area. The well locations and fault numbers are shown in Fig. 1D.



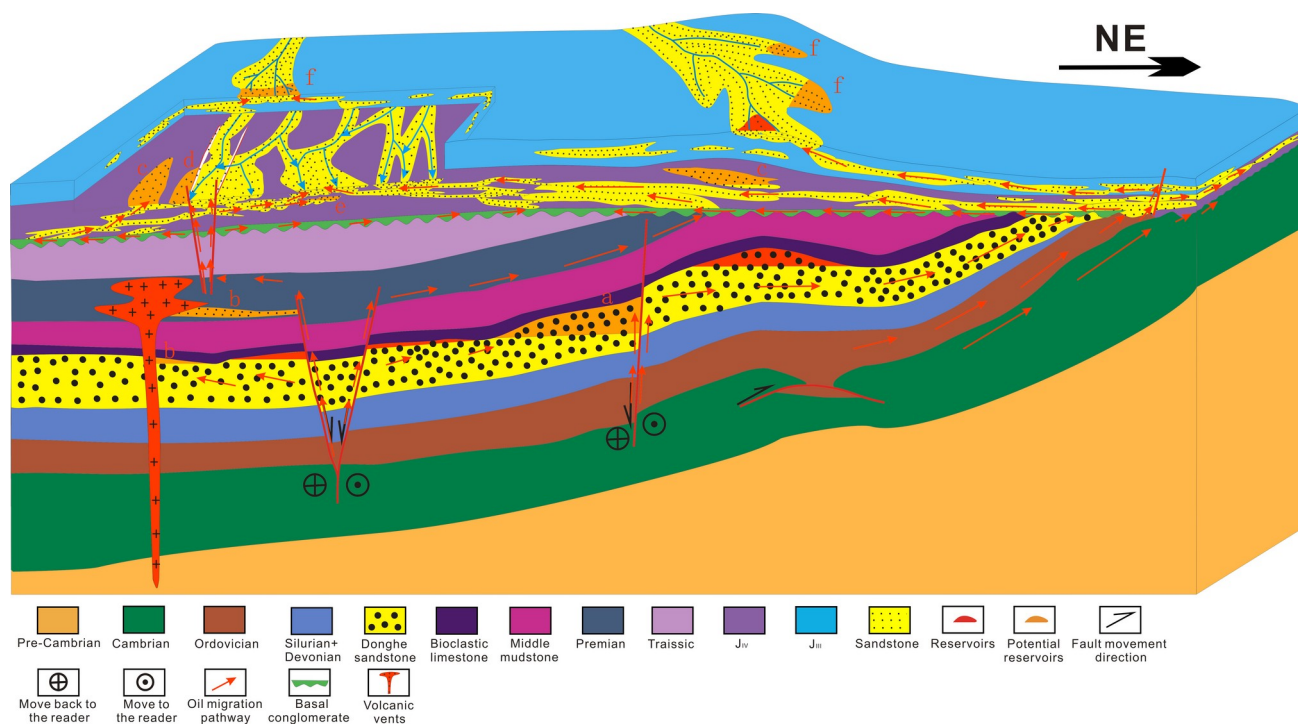


Fig. 14. The model of fault mesh petroleum plays in the study area, not to scale. Please see the text for additional details.

## Tables

Table 1. The oil properties and bulk composition of the Carboniferous Donghe sandstone and the Jurassic.

Strata	Well	Well test results	Depth, meter	Re+Asp ( % )	Wax ( % )	Sul ( % )	Viscosity ( 50℃ ) ( mPa·s )	Density ( 20℃ ) ( g/cm <sup>3</sup> )	Sat (%)	Aro (%)	Re (%)	Asp (%)	Sat/Aro
Donghe Sandstone	DH1	Oil	5726-5746	11.7	4.8	0.7	6.9	0.863	60.2	18.8	12.8	7.9	3.2
			5756-5800	11	7.6	0.7	5.7	0.858					
			5810-5819	12.2	5.25	0.9	12.47	0.882					
	DH1-5-8	Heavy oil	5821-5839	42.53	14.21	1.86	4700	0.9202	53.7	21	5.3	4.4	2.56
	DH11	Oil	5712-5724	25.1	11.9	nd	5.6	0.858					
		Condensate oil	5728-5739					0.763					
	DH13	Heavy oil	5830-5858.5						39.9	5.8	5.4	47.5	6.9
		Bitumen	5871-5886										
	DH1-H4	Oil	5835-6250	11.1	5.3	0.42	6.71	0.8569					
	DH1-H5	Oil	5864-6365	8.48	9.39	0.66	6.939	0.8552	65.8	17.8	7.7	6.7	2.6
	DH1-7-9	Oil	5767-5802	12.45	11.67	0.84	13.29	0.8746	40.1	17.5	8.1	32.6	2.3
	DH1-H18c	Oil	5981-6016	7.77	6.2	0.78	6.227	0.8707	48.2	15.8	8.5	25.7	3.1
	DH1-H17	oil	5948-6348	9.41	4.99	0.71	6.955	0.8571	71.4	14.9	4.7	7	2.6
		Oil	5796-5810	13.8	5.8	0.9	15.2	0.885	38.8	17.8	14.5	27.9	2.2
	DH20	Heavy oil	5958-5970	29.1	nd	nd	5617.11	0.9813					
		Oil	6068-6085	6.5	5.8	0.7	6	0.85					
J <sub>IV</sub>	DH20	Condensate oil	5480-5490	nd	6.4	nd	1.47	0.8172	45.62	16.06	8.03	28.49	2.84
	DH1-5-5	Oil	5483-5488	12.42	7.8	0.8	13.34	0.8769	25	15.67	11.67	47.33	1.6
	DH12	Condensate oil	5483-5491	4.87	3.15	0.24	1.3	0.7994	25.57	25.28	8.81	39.78	1.01
J <sub>III</sub>	DH11	Heavy oil	5440-5450	nd	nd	nd	374.7	0.9478					
	DH20	Condensate oil	5439-5443	0.5	2	1	0.83	0.7651					
		Heavy oil	5446-5454	nd	nd	nd	5600	0.9814					
	DH23	Condensate oil	5436.7-5445	nd	nd	nd	1.18	0.8023					

Re: resin; Asp: asphaltene; Sul: sulfur; Sat: saturated hydrocarbons; Aro: aromatic hydrocarbons; Sat/Aro: the ratio of saturated hydrocarbons to aromatic hydrocarbons; nd, not determined; a blank space means there is no test data.

Table 2. The geochemistry parameters of the Donghe sandstone and the Jurassic reservoirs.

Strata	Well	Sample type	Depth meter	Max peak	CPI	OEP	$\sum C_{21-}/\sum C_{22+}$	Pr/nC <sub>17</sub>	Ph/nC <sub>18</sub>	Pr/Ph	Carbonchain range
Donghe sandstone	DH1	Oil	5766.5	14	0.89	1.05	5.18	0.32	0.42	1	C <sub>12</sub> -C <sub>34</sub>
		Oil	5792	17	0.99	1.27	2.32	0.34	0.4	0.87	C <sub>13</sub> -C <sub>30</sub>
		Oil	5802	14	1.05	1.01	1.61	0.34	0.41	0.89	C <sub>11</sub> -C <sub>34</sub>
		Oil	5811.5	19	1.08	1.06	1.34	0.34	0.4	0.81	C <sub>12</sub> -C <sub>35</sub>
		Oil	5815.5	19	0.99	1	0.85	0.32	0.41	0.49	C <sub>13</sub> -C <sub>36</sub>
		Oil	5825	21	1	1	1.08	0.31	0.38	0.82	C <sub>13</sub> -C <sub>35</sub>
	DH1-H17	Oil	5948-6348	21	1.05	1.04	1.35	0.31	0.41	0.71	C <sub>10</sub> -C <sub>36</sub>
	DH20	Oil	5699.3	26	0.99	0.99	0.17	0.56	0.53	0.65	C <sub>15</sub> -C <sub>38</sub>
		Oil	5704.6	31	1.01	1	0.11	0.89	0.69	0.57	C <sub>16</sub> -C <sub>38</sub>
	DH1-H4	Oil	5835-6240	20	0.98	1	0.85	0.24	0.42	0.32	C <sub>11</sub> -C <sub>36</sub>
	DH1-6-8	Oil	5726-5809	21	1.08	1.06	1.22	0.32	0.42	0.7	C <sub>10</sub> -C <sub>36</sub>
	DH1-7-6	Oil	5483-5488	19	1.02	1.01	1.38	0.38	0.41	0.83	C <sub>14</sub> -C <sub>36</sub>
	DH1-7-9	Oil	5767-5802	18	1.09	1	1.62	0.35	0.43	0.8	C <sub>11</sub> -C <sub>38</sub>
	DH4	Oil	6068-6085	19	1.05	1.05	1.39	0.36	0.36	0.72	C <sub>15</sub> -C <sub>36</sub>
	DH6	Oil	5985-5998	19	1.03	1.04	1.16	0.4	0.46	0.78	C <sub>14</sub> -C <sub>37</sub>
J <sub>IV</sub>	DH20	Oil	5480-5490	19	1.03	1.04	1.16	0.4	0.46	0.78	C <sub>14</sub> -C <sub>37</sub>
	DH1-5-5	Oil	5483-5488	19	1.03	1.04	1.16	0.4	0.46	0.78	C <sub>14</sub> -C <sub>37</sub>
J <sub>III</sub>	DH30	Asphaltic sand	5418.9	20	1.03	0.96	0.86	0.24	0.42	0.33	C <sub>11</sub> -C <sub>36</sub>
		Asphaltic sand	5417.5	19	0.96	0.99	1.04	0.24	0.36	0.44	C <sub>10</sub> -C <sub>36</sub>
		Oil	5424-5426	20	1.1	0.93	1.19	0.31	0.48	0.47	C <sub>10</sub> -C <sub>32</sub>
	DH20	Heavy oil	5444-5451	17	1.04	nd	0.95	0.31	0.38	0.83	C <sub>15</sub> -C <sub>37</sub>
	DH1	Oil sand	5453	19	1	1.06	2.41	0.39	0.38	0.91	C <sub>13</sub> -C <sub>35</sub>
		Oil sand	5455	18	0.91	0.96	2.77	0.41	0.39	0.92	C <sub>13</sub> -C <sub>35</sub>

Oil sand	5465	19	1.11	1.25	2.32	0.39	0.4	0.98	C <sub>12</sub> -C <sub>35</sub>
----------	------	----	------	------	------	------	-----	------	----------------------------------

nd, not determined.

Table 3. The components of natural gas of the Donghe sandstone and the Jurassic

Strata	Well	Depth meter	C <sub>1</sub> ( % )	C <sub>2+</sub> ( % )	CO <sub>2</sub> ( % )	N <sub>2</sub> ( % )	C <sub>1</sub> /C <sub>1+</sub> (%)	Relative density
Donghe sandstone	DH1	5726-5746	39.87	18.7	18.23	21.61	68.1	1.066
		5756-5800	43.92	15.46	19.35	20.98	74	1.009
	DH11	5712-5724	36.98	12.31	26.76	23.95	75	0.805
	DH6	5985-5998	28.88	20.04	23.21	27.87	59.1	1.18
	DH14	6116-6126	23.54	18.48	22.57	35.41	56	1.2
	DH4	6068-6086	23.83	25	20.38	30.64	48.8	1.22
	DH1-5-5	5745-5795	43.24	10.22	22.24	24.3	80.9	0.98
	DH1-H18c	5981-6016	34.5	7.8	31.1	26.6	81.6	1.049
J <sub>IV</sub>	DH20	5480-5490	82.59	11.24	1.75	4.42	88	0.68
J <sub>III</sub>	DH23	5443-5448	83.6	9.84	2.35	3.28	89.5	0.69
	DH20-H3	5542-6073	86.4	8.67	2.08	2.81	90.9	0.65

C<sub>1</sub>, methane; C<sub>2+</sub>, ethane and its heavier components; C<sub>1+</sub>, total hydrocarbon components.

Table 4. The light hydrocarbon parameters of natural gas of the Donghe sandstone and the Jurassic

Strata	Well	Depth,meter	a(%)	b(%)	c(%)	d(%)	e(%)	f	g	k <sub>1</sub>	m	n
Donghe sandstone	DH1-H4	5835-6240	46.2	30.5	10.4	4.02	1.77	2.56	0.79	1.03	0.26	0.59
	DH1-H5	5864-6365	51.8	25.7	14.3	0.07	0.64	5.33	1.27	1.06	0.38	0.63
	DH1-6-8	5726-5809	50.0	27.4	2.6	0.18	0.91	4.98	1.37	1.08	0.37	0.67
	DH1-7-9	5767-5802	48.9	23.8	1.8	0.07	0.33	4.09	1.06	1.12	nd	0.47
	DH1-H17	5948-6348	45.1	19.5	2.1	0.12	0.63	4.86	1.22	1.13	0.39	0.68
	DH6	5985-5998	34.2	12.0	3.8	11.58	4.49	5.6	1.39	1.13	nd	0.39
	DH4-3	6082-6086	21.7	16.4	0.6	0.12	0.12	1.09	0.25	1.10	0.83	0.91
J <sub>IV</sub>	DH20	5480-5490	46.37	33.79	9	3.36	4.44	3.89	1.01	1.07	0.49	0.5
	DH1-5-5	5483-5488	39.04	33.27	14.7	4.02	1.77	2.56	0.79	1.03	0.59	0.54
J <sub>III</sub>	DH20-H1	5650-5973	37.27	26.21	18.9	4.38	13.18	5.85	1.35	1.12	0.42	0.39
	DH30	5424-5426	48.75	35.82	11.04	0.08	0.21	4.17	1.12	1.11	0.46	0.56
	DH20	5444-5451	45.18	32.31	16.07	2.5	3.92	3.53	0.92	1.16	0.7	0.59

Definitions of compositions: a, n-alkanes; b, branched alkanes; c, cycloalkanes; d, benzene; e, toluene; f, 2-methylhexane; g, 2,3-dimethylpentane; k<sub>1</sub>, (2-methylhexane + 2,3-dimethylpentane)/(3-methylhexane + 2,4-dimethylpentane); m, isopentane/n-pentane; n, isohexane/n-hexane